Spatial and seasonal variability in volatile organic sulfur compounds in seawater and the overlying atmosphere of the Bohai and Yellow Seas

Juan Yu[1,2,3,†], Lei Yu[1,†], Zhen He[1,2,3], Gui-Peng Yang[1,2,3,*], Jing-Guang Lai[1], Qian Liu[1]

[1]Frontiers Science Center for Deep Ocean Multispheres and Earth System, Key Laboratory of Marine Chemistry Theory and Technology, Ministry of Education, Ocean University of China, Qingdao 266100, China.

[2]Laboratory for Marine Ecology and Environmental Science, Qingdao National Laboratory for Marine Science and Technology, Qingdao 266237, China.

[3]Institute of Marine Chemistry, Ocean University of China, Qingdao 266100, China.

Abstract. Volatile organic sulfur compounds (VSCs), including carbon disulfide (CS_2), dimethyl sulfide (DMS), and carbonyl sulfide (COS), were surveyed in the seawater of the Bohai and Yellow Seas and the overlying atmosphere during spring and summer of 2018 to understand the production and loss of VSCs and their influence factors. The concentration ranges of COS, DMS, and CS_2 in the surface seawater were 0.14–0.42, 0.41–7.74, and 0.01–0.18 nmol L^{-1} during spring and 0.32–0.61, 1.31–18.12, and 0.01–0.65 nmol L^{-1} during summer, respectively. The COS concentrations exhibited positive correlation with dissolved organic carbon (DOC) concentrations in seawater during summer, which verified the photochemical production of COS from chromophoric dissolved organic matter (CDOM). High DMS concentrations occurred near the Yellow River, Laizhou Bay, and Yangtze River Estuary, coinciding with high nitrate and Chl a concentrations due to river discharge during summer. The COS, DMS, and CS_2 concentrations were the highest in the surface seawater and decreased with the depth. The mixing ratios of COS, DMS, and CS_2 in

---

* Corresponding author at: Key Laboratory of Marine Chemistry Theory and Technology, Ministry of Education, Ocean University of China, 238 Songling Road, Qingdao 266100, China. E-mail address: gpyang@mail.ouc.edu.cn (G.-P. Yang)

†These authors contributed equally to this work and should be considered co-first authors.

the atmosphere were 255.9–620.2 pptv, 1.3–191.2 pptv, and 5.2–698.8 pptv during spring and 394.6–850.1 pptv, 10.3–464.3 pptv, and 15.3–672.7 pptv in summer, respectively. The mean oceanic concentrations/atmospheric mixing ratios of COS, DMS, and CS_2 were 0.8/0.6-, 2.1/3.6-, and 2.7/0.5-fold higher in summer than in spring. The mean sea-to-air fluxes of COS, DMS, and CS_2 were 0.2-, 1.1-, and 3.3-fold higher in summer than in spring. The sea-to-air fluxes of VSCs indicated that these marginal seas are major sources of VSCs in the atmosphere. The results provide help with a better understanding of the contribution of VSCs in marginal seas.

1 Introduction

Carbonyl sulfide (COS), dimethyl sulfide (DMS), and carbon disulfide (CS_2) are three major volatile organic sulfur compounds (VSCs) in seawater and the marine atmosphere. Their biogeochemical cycles are closely related to climate change (Charlson et al., 1987; Li et al., 2022). VSCs contribute to the formation of atmospheric cloud condensation nuclei (CCN) and sulfate aerosols, significantly affecting the global radiation budget and ozone concentration (Andreae and Crutzen, 1997). Hence, interest in the distribution, production, and chemistry of VSCs has grown in recent years (Lennartz et al., 2017; Lennartz et al., 2020; Li et al., 2022; Remaud et al., 2022; Whelan et al., 2018; Yang et al., 2008; Yu et al., 2022).

COS has an average tropospheric residence time of 2–7 years and is the most abundant and widely distributed reduced sulfur trace gas in the atmosphere (Brühl et al., 2012). COS can be converted to sulfate aerosols in the stratosphere, affecting the Earth's radiation balance (Crutzen, 1976). Atmospheric COS originates directly from oceanic emissions and indirectly from the oxidation of DMS and CS_2 (Kettle et al., 2002; Lennartz et al., 2020). Uptake by terrestrial vegetation and soil is the most important sink of atmospheric COS (Kettle et al., 2002; Maignan et al., 2021). Therefore, COS can be used as a proxy for estimating the photosynthesis rate in ecosystems (Campbell et al., 2008). COS production is dependent on UV radiation, chromophoric dissolved organic matter (CDOM), cysteine, and nitrate concentration (Lennartz et al., 2021; Li et al., 2022). COS production rates increase with increasing nitrate concentration (Li et al., 2022). Some studies have indicated that the ocean is a COS source (Chin and Davis, 1993; Yu et al., 2022), whereas others have shown that the ocean is a COS sink (Zhu et al., 2019).

Atmospheric DMS can react with OH and NO_3 radicals to form SO_2 and methane sulfonic acid (MSA, CH_3SO_3H), creating non-sea salt sulfates (nss-SO_4^{2-}), which contribute to acid deposition and CCN (Charlson et al., 1987). DMS is the predominant biogenic sulfur originating from dimethylsulfoniopropionate (DMSP), predominantly produced by bacteria and phytoplankton (Curson et al., 2017; Keller et al., 1989). DMSP lyase from phytoplankton and bacteria can convert DMSP to DMS (Reisch et al., 2011). The community composition of phytoplankton and bacteria can affect the net DMSP concentrations via synthesis and degradation (O'Brien et al., 2022, Zhao et al., 2021). DMS

52 entering the atmosphere via sea-to-air exchange accounts for about 50% of all natural sulfur releases (Cline and Bates,

53 1983).

54 CS$_2$ is the key precursor of COS, and 82% COS is the oxidation production of CS$_2$ (Lennartz et al., 2020).

55 Photochemical reaction with dissolved organic matter (DOM) is a principal source of CS$_2$ in seawater (Xie et al.,

56 1998). ^{3}CDOM*, ^{1}O$_2$, H$_2$O$_2$, and $^{\bullet}$OH produced by the photochemical reaction of DOM react with DMS and produce

57 COS and CS$_2$ (Modiri Gharehveran and Shah, 2021). Anthropogenic CS$_2$ sources include rayon and/or aluminum

58 production, fuel combustion, oil refineries, and coal combustion (Campbell et al., 2015; Zumkehr et al., 2018).

59 Two different approaches (ice core and isotope measurements) were used to evaluate anthropogenic COS emissions

60 (Aydin et al., 2020; Hattori et al., 2020). The latter study and a modeling approach used by Remaud et al. (2022)

61 observed a gradient of anthropogenic COS in East Asia. Anthropogenic COS is initially emitted as CS$_2$ and oxidized

62 by OH to COS in the atmosphere (Kettle et al., 2002). The production and loss of DMS involve phytoplankton and

63 bacteria synthesis, zooplankton grazing, bacterial degradation, and sea-air diffusion (Schäfer et al., 2010). COS and

64 CS$_2$ production are related to photo-oxidation and/or photochemical reactions (Lennartz et al., 2020; Xie et al., 1998).

65 However, the production and loss mechanisms remain unclear.

66 Yu et al. (2022) investigated the distributions of COS, DMS, and CS$_2$ and sea-to-air flux in the Changjiang Estuary

67 and the adjacent East China Sea, demonstrating that oceanic VSCs (COS, DMS, and CS$_2$) are sources of atmospheric

68 VSCs. In contrast, Zhu et al. (2019) showed that the ocean was a COS sink. The Yellow Sea (YS) and Bohai Sea (BS)

69 are semi-enclosed seas in the northwestern Pacific Ocean. The BS coastal current, YS coastal current, and YS warm

70 current substantially affect the hydrological characteristics of this area (Chen, 2009), potentially altering the VSC

71 distributions via water mass exchanges. In addition, the Yellow Sea Cold Water Mass (YSCWM), a seasonal

72 hydrological phenomenon located in the 35 °N transect, forms, peaks, and disappears in spring, summer, and after

73 September, respectively (Zhang et al., 2014). In this study, we investigate the spatial distributions and seasonal

74 variability of COS, DMS, and CS$_2$ in the seawater and overlying atmosphere of the YS and BS and the effects of the

75 YSCWM (the 35 ˚N transect) on the VSC distributions to better understand the distributions and impact factors of

76 VSCs in Chinese marginal seas.

2 Materials and methods

2.1 Sampling

79 Two cruises were conducted aboard the R/V "Dong Fang Hong 2" in the YS and BS from 27 March to 16 April

80 (spring) 2018 and from 24 July to 8 August (summer) 2018. The sampling stations are shown in Fig. 1. Seawater

81 samples were collected using 12 L Niskin bottles mounted on a Seabird 911 conductivity-temperature-depth (CTD)

82 rosette. The seawater was slowly siphoned from the Niskin bottles into 100 mL glass jaw bottles (CNW Technologies

83 GmbH, GER) via a translucent silicone tube. The seawater was allowed to overflow the sampling bottle by twice its

84 volume before the silicone tube was gently removed, and the bottle was immediately sealed with an aluminum cap

85 containing a Teflon-lined butyl rubber septum without any headspace. Subsequently, the concentrations of oceanic

86 VSCs were immediately measured on the ship. The environmental and hydrological parameters such as seawater

87 temperature and salinity were measured simultaneously by the CTD equipment.

88 Atmospheric VSC samples were collected using cleaned and vacuumed SilcoCan canisters (Restek, USA) in the

89 windward direction approximately 10 m above the ocean. The stability of VSCs in fused silica-lined canisters has

90 been verified during storage for 16 d at room temperature (Brown et al., 2015). The atmospheric samples were

91 analyzed immediately after being brought back to the laboratory.

2.2 Analytical procedures

93 The VSC concentrations in the seawater were measured using a gas chromatograph (GC) (Agilent 7890A, USA) with

94 a flame photometric detector (FPD). The atmospheric VSC mixing ratios were measured using a GC equipped with a

95 mass spectrometer (GC-MS) (Agilent 7890A/5975C, USA) using the methods of Inomata et al. (2006) and Staubes

96 and Georgii (1993), respectively. A CP-Sil 5 CB column (30 m $\times$ 0.32 mm $\times$ 4.0 μm, Agilent Technologies, USA)

97 was used to separate the three VSCs. Standard VSC gases with mixing ratios of 1 ppmv were bought from Beijing

98 Minnick Analytical Instrument Equipment Center. Qualitative analysis was conducted by comparing the results with

99 the retention times of the standards, and quantitative analysis was conducted by diluting the VSC standard gases to 1

ppbv and 5 ppbv using a 2202A dynamic dilution meter (Nutech, USA) and injecting different volumes of the diluted VSC standards into the GC using a gas-tight syringe. The VSC mixing ratios were calculated after calibration using standard gases (Fig. S1).

The VSC concentrations in seawater were determined using a cryogenic purge-and-trap system coupled with the GC-FPD. A 30 mL seawater sample was injected into a glass bubbling chamber with a gas-tight syringe (SGE, Australia). The VSCs were extracted from the seawater with high purity N_2 at a rate of 60 mL min^{-1} for 15 min and passed through an anhydrous $CaCl_2$-filled drying tube and a 100% degreased cotton-filled 1/4 Teflon tube to remove water and oxides. Subsequently, the VSC gases were passed through a six-way valve and trapped in a loop of the 1/16 Teflon capture tube immersed in liquid nitrogen. After all VSCs had been purged from the seawater, the capture tube was removed from the liquid nitrogen and placed into hot water (> 90 ℃) to desorb the trapped VSCs. The VSCs gases were carried into the GC by N_2 and detected by the FPD. The column temperature was programmed with an initial temperature of 55 ℃, followed by an increase to 100 ℃ at 10 ℃ min^{-1} and a final increase to 150 ℃ at 15 ℃ min^{-1}. The inlet and detector temperatures were 150 ℃ and 160 ℃, respectively, and the split ratio of pure N_2 was 10:1. The detection limits of the method for COS, DMS, and CS_2 were 33 pg, 387 pg, and 22 pg and the measurement precision was 5.59%-11.70% (Tian et al., 2005). The DMS concentrations in seawater were obtained from Zhang et al. (2023).

The mixing ratios of atmospheric VSCs were analyzed using an Entech 7100 pre-concentrator (Nutech, USA) coupled with GC-MS. The sample SilcoCan canister was connected to the pre-concentrator, and 200 mL of gas was drawn into the preconcentration system with a three-stage cold trap (Fig. S1). The pre-concentrator parameters of the three-stage cold trap are listed in Table S1. The first trap removes N_2, O_2, and H_2O (g) from the atmospheric samples, and the second trap eliminates CO_2. The third trap is used to separate the three VSCs and obtain better peak shapes. The temperature programming of the column was the same as for the seawater samples. In addition, the temperature of the quadrupole and ion source were 110 ℃ and 230 ℃, respectively, and the electron ionization source was run at 70 ev. The carrier gas had a split ratio of 10:1 and a flow rate of 2.0 mL min^{-1}. Qualitative and quantitative analyses of the VSCs were conducted using the full scan mode (SCAN) and the selected ion monitoring mode (SIM). The mass-to-charge ratios (m/z) for COS, DMS, and CS_2 were 60, 62, and 76, respectively. The detection limit of the VSCs was 0.1-0.5 pptv (Zhu et al., 2017).

2.3 Calculation of sea-to-air fluxes of VSCs

127   The sea-to-air fluxes of the VSCs were calculated using the model established by Liss and Slater (1974): $F = k_w(c_w -$

128    $c_g/H)$, where F is the sea-to-air flux of VSCs (μmol m^{-2} d^{-1}); k_w is the VSC transfer velocity (m d^{-1}); c_w and c_g are the

129   equilibrium concentrations of VSCs in the surface seawater and the atmosphere (nmol L^{-1}), respectively; and H is

130   Henry's constant calculated using the equation listed in Table S2 (De Bruyn et al., 1995; Dacey et al., 1984). It was

131   converted to a dimensionless constant using the equation proposed by Sander (2015). k_w was calculated from the wind

132   speed, and the sea surface temperature was obtained by the N2000 method (Nightingale et al., 2000). This method has

133   been internationally accepted; we used the calculation developed by Kettle et al. (2001).

134   **2.4 Measurements of Chl *a*, nutrients, and dissolved organic carbon**

135   The seawater samples for the analysis of the Chl *a* concentrations were filtered through Whatman GF/F filters, and

136   the filtrate was stored in darkness at −20 °C. Then, Chl *a* was extracted with 90% acetone for 24 h at 4 °C in darkness.

137   The Chl *a* concentrations were determined following the method of Parsons et al. (1984) with a fluorescence

138   spectrophotometer (F-4500, Hitachi) at excitation/emission wavelengths of 436 nm/670 nm. The seawater was filtered

139   through Whatman GF/F filters (0.7 μm), and the filtered water samples were stored at −20 °C before nutrient (nitrate,

140   phosphate, and silicate) analysis. A Technicon Autoanalyser AAII (SEAL Analytical, UK) was used to measure the

141   nitrate, phosphate, and silicate concentrations. The nitrate, phosphate, and silicate data were provided by the open

142   research cruise supported by the National Natural Science Foundation (NSFC) Shiptime Sharing Project.

143   The dissolved organic carbon (DOC) concentrations were measured using the method of Chen et al. (2021). The

144   seawater was filtered through Whatman GF/F filters (pre-combusted at 500 °C for 4 h), and the filtrate was stored at

145   −20 °C for DOC analysis. The DOC concentrations were determined by a total organic carbon analyzer (Shimadzu

146   TOC-VCPH) after adding two drops of 12 mol/L HCl.

147   **2.5 Data analysis**

148   SPSS 24.0 software (SPSS Inc., Chicago, IL, USA) was used to analyze the relationships between the environmental

149   factors and the concentrations and mixing ratios of the three VSCs in seawater and the atmosphere during spring and

150   summer.

151   **3 Results**

3.1 Spatial distributions of COS, DMS, and CS$_2$ in surface seawater

3.1.1 Spring distributions

The temperature in the surface seawater showed a decreasing trend from south to north, and the salinity increased from the inshore to the offshore sites due to the influences of the YS warm current, Yalu River, and Yellow River (Fig. 2). The Chl *a* concentrations in the surface water of the BS and YS in the spring were 0.17–4.45 µg L^{-1} with an average of 1.19 ± 0.96 µg L^{-1}. The highest Chl *a* concentration occurred at station B39 in the BS (Fig. 2), which may be related to the enhanced phytoplankton growth due to the abundance of nutrients resulting from a seawater exchange between the BS and YS. In addition, high Chl *a* concentrations were observed in the central area of the southern YS.

The concentrations of COS, DMS, and CS$_2$ in the surface seawater of the BS and YS during spring were 0.14–0.42, 0.41–7.74, and 0.01–0.18 nmol L^{-1}, with mean values of 0.24 ±0.06, 1.74 ±1.61, and 0.07 ±0.05 nmol L^{-1}, respectively (Fig. 2). The high COS concentrations during the spring occurred in the YS (Fig. 2). The highest COS concentration was observed at station H21, coinciding with a high Chl *a* concentration. The two areas with high concentrations of COS in the central waters of the southern YS overlapped with areas with high Chl *a* concentrations. High DMS concentrations existed in the coastal waters of the southern Shandong Peninsula, as well as at station B21 in the central part of the northern YS. The distribution of CS$_2$ in seawater exhibited a decreasing trend from inshore to offshore (Fig. 2). High CS$_2$ concentrations appeared at stations H18 and H19 in the coastal waters of YSCWM (Fig. 2). There was also a high CS$_2$ concentration at station B30 near the shore of the Liaodong Peninsula (Fig. 2).

3.1.2 Summer distributions

The temperature and salinity in the BS and YS in summer were relatively high, and high Chl *a* concentrations were concentrated in coastal waters (Fig. 3). The Chl *a* concentrations in the seawater during summer were 0.10–4.74 µg L^{-1} with an average of 1.60 ± 1.19 µg L^{-1}. Station B43 near the Yellow River estuary and Laizhou Bay had the highest Chl *a* concentration, which may have been due to the abundance of nutrients (nitrate: 5.85 µmol L^{-1}, silicate: 17 µmol L^{-1}) carried by nearby rivers or coastal currents (Figs. 3 and S2). Low salinities and high nitrate and Chl *a* concentrations occurred at Stations H32, H34, and H35 in the northeast of the Yangtze River Estuary and at Stations B66 and B68 near the Laizhou Bay and Yellow River Estuary (Figs. 3 and S2).

8

177   The concentrations of COS, DMS, and CS_2 in the surface water of the BS and YS during summer were 0.32–0.61,

178   1.31–18.12, and 0.01–0.65 nmol L^{-1}, with mean values of 0.44 $\pm$ 0.06, 5.43 $\pm$ 3.60, and 0.26 $\pm$ 0.15 nmol L^{-1},

179   respectively (Fig. 3). The mean concentrations of Chl a, COS, DMS, and CS_2 were 0.3-, 0.8-, 2.1-, and 2.7-fold higher

180   in summer than in spring. High COS concentrations were observed at stations B38 and B54 in the BS during summer.

181   In addition, COS had a high concentration at station H25 in the central part of the southern YS, close to a location

182   with a high CS_2 concentration (Fig. 3). High DMS concentrations were common in the northern BS and were generally

183   coincident with high Chl a levels. However, high Chl a and DMS concentrations were found in the coastal waters of

184   the Yangtze River Estuary due to the Changjiang diluted water. In addition, the DMS concentration was high at station

185   H12 (Fig. 3). There were high CS_2 concentrations in the northeastern area of the Yangtze River estuary (Fig. 3).

186   **3.2 Depth distributions of COS, DMS, and CS_2 in seawater**

187   **3.2.1 Depth distributions in spring**

188   The temperature and Chl a decreased from the surface to the bottom seawater (Fig. 4). The mean concentrations of

189   Chl a, COS, DMS, and CS_2 were 4.4-, 4.1-, 4.9-, and 7.9-fold higher at the surface (~ 4 m depth) than at greater depths

190   (> 60 m) (Fig. 4). Consistent with the Chl a distribution, the depth distribution of DMS in the seawater decreased

191   from the euphotic zone to the bottom seawater (Fig. 4). High COS concentrations occurred in the surface seawater

192   and decreased with the depth, and the lowest concentrations occurred in the bottom waters. CS_2 exhibited depth

193   gradients at most stations during spring, with higher concentrations at the surface, except for station H15 where the

194   CS_2 concentrations were high in the bottom seawater.

195   **3.2.2 Depth distributions in summer**

196   The YSCWM affected the depth distributions in summer in the 35 °N transect. Substantial temperature differences

197   occurred between the surface and bottom seawater in summer, and stratification in the water bodies was observed (Fig.

198   5). A distinct thermocline existed at a depth of 20 m, indicating the formation of the YSCWM (Fig. 5). All high Chl

199   a concentrations in the surveyed area of the BS and YS during summer occurred in the euphotic zone, and the highest

200   concentrations occurred in waters at depths of 10–20 m (Fig. 5). The mean Chl a concentrations were 4.4-fold higher

201   at depths of 10–20 m than at depths > 60 m. The depth distribution of DMS in seawater during summer decreased

202   from the surface to the bottom seawater (Fig. 5). A significant depth gradient in the COS and CS_2 concentrations

203   occurred at most stations, exhibiting decreases with the increasing depth. The mean concentrations of COS, DMS, and

204   CS_2 were 11.0-, 7.6-, and 10.5-fold higher at the surface (~ 3 m) than at depths > 60 m. However, the COS

205   concentration was high in the bottom waters of station H16 (0.465 nmol L^{-1}) (Fig. 5). The mean concentrations of Chl

206   *a*, COS, DMS, and CS_2 of all samples at different depths were 1.2-, 0.0-, 4.6-, and 1.0-fold higher or equal to those in

207   summer (1.34 μg L^{-1}, 0.20 nmol L^{-1}, 4.38 nmol L^{-1}, and 0.158 nmol L^{-1}, respectively) than in spring (0.61 μg L^{-1}, 0.20

208   nmol L^{-1}, 0.78 nmol L^{-1}, and 0.080 nmol L^{-1}, respectively).

209   3.3 VSCs in the atmosphere

210   3.3.1 Spring

211   The mixing ratios of COS, DMS, and CS_2 in the atmosphere overlying the BS and YS in spring were in the ranges of

212   255.9–620.2 pptv, 1.3–191.2 pptv, and 5.2–698.8 pptv (Figs. 6a-6c), and their mean mixing ratios were 345.6 ±79.2

213   pptv, 47.5 ±49.8 pptv, and 113.2 ±172.3 pptv, respectively. The decreasing order of the mean mixing ratios of the

214   three VSCs in the atmosphere during spring was COS > CS_2 > DMS. The highest mixing ratio of atmospheric COS

215   occurred at station B72 (Fig. 6a) near the northern Shandong Peninsula. The highest atmospheric DMS mixing ratio

216   was observed at station B08 (Fig. 6b). The DMS concentration in the seawater (Fig. 2) was not as high as that in the

217   atmosphere at station B49 (Fig. 6b). According to the 72 h backward trajectory map (Fig. S3), the air mass over station

218   B49 had migrated from the land to the ocean, passing through Beijing, Tianjin, and other densely populated areas.

219   The air mass over station B47 was slightly different from that of station B49, and the distance across the ocean was

220   shorter than that of B49 and passed over land (Fig. S3). The lowest atmospheric DMS mixing ratio was observed at

221   station B47 (Fig. 6b), probably due to the low DMS concentration in seawater (0.5 nmol L^{-1}) and the loss across the

222   land. The highest atmospheric DMS mixing ratio occurred at station B08 (Fig. 6b); high oceanic DMS concentrations

223   at or near stations where air masses were passing through (such as station H05) may be the reason (Figs. 2 and S3). In

224   addition, there were high mixing ratios of CS_2 at stations in the BS, such as B57, B60, and B72, and low mixing ratios

225   at stations B17 and B21 in the northern YS (Fig. 6c).

226   3.3.2 Summer

227   The mixing ratios of COS, DMS, and CS_2 in summer ranged from 394.6 to 850.1 pptv, from 10.3 to 464.3 pptv, and

228   from 15.3 to 672.7 pptv, with mean values of 563.8 ± 168.9 pptv, 216.6 ± 136.0 pptv, and 164.4 ± 225.5 pptv,

229   respectively (Fig. 6d-6f). The order of the three VSCs in terms of the mean mixing ratios in the atmosphere during

230   summer was COS > DMS > CS_2. The mean mixing ratios of atmospheric COS, DMS, and CS_2 were 0.6-, 3.6-, and

231   0.5-fold higher in summer than in spring. The three VSCs in the atmosphere over the BS and YS had similar spatial

232   distributions. COS and DMS exhibited the highest mixing ratios at station B64 (Fig. 6d and 6e). The highest mixing

233   ratio of CS_2 in summer appeared at station B49 near the shore, and the lowest one occurred far from shore at station

234   H09 (Fig. 6f). The air masses over stations B49, B64, and H09 had migrated from the land, land, and ocean,

235   respectively (Fig. S3). The distributions of CS_2 showed a decreasing trend from inshore to offshore (Fig. 6f).

236   **3.4 Relationships between environmental factors and COS, DMS, and CS₂ concentrations**

237   A significant correlation was found between the DMS and CS_2 concentrations in the surface seawater in spring ($P <$

238   0.05) and summer ($P < 0.01$) (Table 1). A positive correlation occurred between the COS and DOC concentrations in

239   seawater ($P < 0.05$) and between the CS_2 and Chl a concentrations in seawater ($P < 0.05$) during summer (Table 1).

240   There was a significant correlation between the atmospheric COS and CS_2 mixing ratios in spring and summer ($P <$

241   0.01, Table 1).

242   **3.5 Sea-to-air fluxes of VSCs**

243   **3.5.1 Spring**

244   The sea-to-air fluxes of COS, DMS, and CS_2 in spring were 0.03–1.59, 0.06–25.40, and 0.003–0.30 µmol m^{-2} d^{-1}, with

245   averages of 0.50 ± 0.38, 2.99 ± 4.24, and 0.09 ± 0.08 µmol m^{-2} d^{-1}, respectively (Fig. 7). The highest COS sea-to-air

246   flux was observed at station B36, which had a high wind speed (11.3 m s^{-1}). In comparison, the lowest COS sea-to-air

247   flux occurred at station B12, where the minimum wind speed occurred (1.5 m s^{-1}). The lowest sea-to-air fluxes of

248   DMS and CS_2 occurred at stations H01 and B41 (Fig. 7), where the wind speeds were 0.4 m s^{-1} and 2 m s^{-1}, respectively.

249   The highest DMS and CS_2 sea-to-air fluxes appeared at stations HS4 and B68, respectively, due to high wind speeds

250   and high DMS and CS_2 concentrations in seawater (Fig. 7). A significant correlation was found between the sea-to-

251   air fluxes of COS, DMS, and CS_2 and the wind speeds ($P < 0.01$).

3.5.2 Summer

The sea-to-air fluxes of COS, DMS, and CS_2 in summer were 0.06–1.51, 0.10–25.44, and 0.02–0.99 μmol $m^{-2} d^{-1}$, with averages of 0.60 ± 0.59, 6.26 ± 6.27, and 0.39 ± 0.42 μmol $m^{-2} d^{-1}$, respectively, (Fig. 8). The mean sea-to-air fluxes of COS, DMS, and CS_2 in summer were 0.2-, 1.1-, and 3.3-fold higher than those in spring. Consistent with their order in seawater, the order of the sea-to-air fluxes of the VSCs was DMS > COS > CS_2. The lowest sea-to-air fluxes of COS, DMS, and CS_2 in summer occurred at stations B64, B05, and B57, which had the low wind speeds of 1 m s^{-1}, 0.4 m s^{-1}, and 1.1 m s^{-1}, respectively and low seawater VSC concentrations. The highest sea-to-air flux of COS and DMS occurred at stations B70 and H14, respectively, coinciding with high wind speeds and high COS and DMS concentrations in seawater (Fig. 8). The maximum CS_2 sea-to-air flux appeared at station H09, where the concentration of CS_2 in seawater was 0.31 nmol L^{-1} (Fig. 8). A significant correlation was found between the sea-to-air fluxes of COS, DMS, and CS_2 and the wind speeds ($P < 0.05$).

4 Discussion

4.1 Spatial and depth distributions and seasonal variations in VSCs in seawater

4.1.1 Spatial distributions of VSCs and the impact factors

The COS concentrations in this study were similar to those in six tidal European estuaries (Scheldt, Gironde, Rhine, Elbe, Ems, and Loire) (0.22 nmol L^{-1}) (Sciare et al., 2002), the DMS concentrations were lower than previous observations in the BS and YS in autumn (3.92 nmol L^{-1}) (Yang et al., 2014), and the CS_2 concentrations were lower than those in the coastal waters off the eastern coast of the United States (0.004–0.51 nmol L^{-1}) (Kim and Andreae, 1992). Besides, the VSC concentrations in the seawater of the BS and YS were significantly higher than those in oceanic areas, such as the North Atlantic Ocean (Simó et al., 1997; Ulshöfer et al., 1995). Zepp and Andreae (1994) also showed that the COS concentrations were 40-fold higher in nearshore waters than in the open sea. The higher CDOM concentrations in the nearshore waters may be the reason for the difference (Gueguen et al., 2005). Our results showed that the average COS, DMS, and CS_2 concentrations in the surface seawater of the BS and YS during summer were higher than those in the Changjiang estuary and the adjacent East China Sea (Yu et al., 2022). The reasons may

276   be different sea areas, temperatures, and industrial production. For example, rayon production is the main source of

277   anthropogenic CS_2 (Campbell et al., 2015) in the northern cities of the BS.

278   Different production and consumption mechanisms resulted in different spatial distributions of COS, DMS, and

279   CS_2. DMS and DMSP concentrations are related to the composition and abundance of phytoplankton (Kurian et al.,

280   2020; Naik et al., 2020; O'Brien et al., 2022; Yu et al., 2023). The highest DMS concentrations at station B21 in spring

281   coincided with high Chl a concentrations (Fig. 2). Low salinities ($<$ 30) occurred at stations H25, H26, H34, H35,

282   B43, B66, and B68 due to river water discharge from the Yangtze River Estuary, Yellow River, and Laizhou Bay in

283   summer, consistent with the high nitrate, silicate, Chl a, and DMS concentrations (Figs. 3 and S2). High CS_2

284   concentrations in the coastal waters of the Yellow River estuary and at stations H18, H19, and B30 in spring may be

285   due to high CDOM carried by the YS coastal current and Yellow River and terrestrial input. The significant correlation

286   between the DMS and CS_2 concentrations in the surface seawater was consistent with the results of Ferek and Andreae

287   (1983) and Yu et al. (2022). DMS in seawater is primarily derived from the degradation of DMSP, which is released

288   from algal cell lysis (O'Brien et al., 2022). Moreover, the algae decay increased the CS_2 emission rate due to the

289   degradation of sulfur-containing amino acids (Wang et al., 2023). The commonality of their sources resulted in a high

290   correlation between the DMS and CS_2 concentrations in seawater. Xie et al. (1998) pointed out that CS_2 has a

291   photochemical production mechanism similar to that of COS. Both are primarily produced by photochemical reactions

292   of thiol-containing compounds, such as methyl mercaptan (MeSH) or glutathione, under the catalysis of CDOM.

293   Terrestrial CDOM has higher photochemical reactivity and is more conducive to the photochemical generation of CS_2

294   (Xie et al., 1998). COS production rates increase with an increase in the absorption coefficient at 350 nm (a_{350}) (Li et

295   al., 2022). Uher and Andreae (1997) showed that the COS concentration in seawater was significantly correlated with

296   the CDOM concentration. The positive correlation between the COS and DOC concentrations in seawater during

297   summer in this study suggested that COS was produced by the photochemical reaction of CDOM. COS and CS_2 are

298   formed via a reaction between cysteine and intermediates (e.g., CDOM·, ·OH) (Chu et al., 2016; Du et al., 2017;

299   Modiri Gharehveran et al., 2020). Modiri Gharehveran and Shah (2021) showed that DOM could photochemically

300   produce $^3CDOM^*$, $^1O_2$, H_2O_2, and ·OH by sunlight reacting with DMS, forming a sulfur- or carbon-centered radical

301   and subsequently COS and CS_2. Li et al. (2022) demonstrated that a high nitrate concentration resulted in a high COS

302   production rate. The high COS concentrations at stations H25 and B43 during summer coincided with high nitrate

303   concentrations (Figs. 3 and S2). However, no significant correlations were found between the COS and nitrate

304   concentrations during summer (Tables 1).

305   **4.1.2 Depth distributions of VSCs and impact factors**

306   The depth distributions of DMS, COS and CS_2 showed similar patterns; their concentrations decreased with increasing

307   depth, in agreement with the results of Yu et al. (2022). Yu et al. (2023) also showed that the DMS concentrations in

308   the 35 °N transect of the BS and YS in autumn decreased with an increase in seawater depth. The highest Chl *a*

309   concentrations during summer occurred at depths of 10–20 m. This result was attributed to the abundance of nutrients

310   and suitable water temperatures near the thermocline, benefitting phytoplankton growth. Yu et al. (2021) reported that

311   the highest DMSP-consuming bacterial abundance and DMSP lyase activity at the 35 °N transect in the summer of

312   2013 occurred at depths of 10-15 m, consistent with our Chl *a* concentrations. DMS originates primarily from

313   phytoplankton; thus, its concentration trend is similar to that of Chl *a*. COS and CS_2 in seawater are predominantly

314   derived from photochemical reactions of organic sulfides catalyzed by CDOM; therefore, light is the limiting factor

315   for their production in seawater (Uher and Andreae, 1997). Ulshöfer et al. (1996) studied the depth distribution of

316   COS in seawater and found that high COS concentrations occurred in the euphotic zone. The high COS concentrations

317   in the surface seawater in spring in this study may be attributed to the photochemical production reactions of CS_2 and

318   COS in the euphotic zone because they are dependent on light (Flöck et al., 1997; Xie et al., 1998). The addition of

319   photosensitizers-natural DOM and commercial humic acid (HA) photo-catalyzed glutathione (GSH) and cysteine, and

320   enhanced the COS formation (Flöck et al., 1997). An excited triplet state CDOM (^{3}CDOM*) is produced by COS in

321   the presence of ultraviolet light (Li et al., 2022). Hobe et al. (2001) stated that the non-photochemical production of

322   COS is critical for the global budget. Consistent with Hobe et al. (2001), the high COS concentration in the bottom

323   waters at station H16 in summer may be related to the non-photochemical production of COS or release by underlying

324   sediments. Consistent with our CS_2 results, Xie et al. (1998) showed that the CS_2 concentrations decreased with the

325   depth, coinciding with solar radiation changes. Decreased photochemical reaction due to decreasing solar radiation

326   with water depth may explain the vertical distribution of CS_2 (Xie et al., 1998). Similar to the results of Xie et al.

327   (1998), the high CS_2 concentrations in the bottom seawater at station H15 in spring may be attributable to a

328   sedimentary source.

329   **4.1.3 Seasonal and diurnal variations in VSCs in seawater**

330   The VSCs in seawater exhibited significant seasonal differences (VSCs in summer > VSCs in spring) in this study.

331   Similar seasonal variations in COS were also observed by Xu et al. (2001), who found that the COS concentrations in

332   South Africa were higher in summer than in autumn. In addition, observations by Weiss et al. (1995) showed that the

333   COS concentrations in the seawater of the Atlantic and Pacific Oceans were very low in winter. Xu et al. (2001)

334   concluded that warmer seasons and high biological productivity resulted in enhanced COS concentrations. The

335   significant correlation between the oceanic COS concentrations and the temperatures in spring (Table 1) can prove

336   this. Xie et al. (1998) showed that the order of the CS_2 production rates was summer > spring> fall > winter. The

337   significant positive correlations between the CS_2 and Chl a concentrations during summer may explain the higher CS_2

338   concentration in seawater during summer than during spring in this study. Similar to the seasonal changes in Chl a,

339   the DMS concentrations were higher in summer than in spring. A higher phytoplankton biomass in summer has been

340   linked to higher DMS concentrations in summer than in autumn (Yang et al., 2015).

341   In addition, diurnal variations in the COS concentrations in seawater (high during the daytime and low at night)

342   were reported (Xu et al., 2001; Ferek and Andreae, 1984). COS photoproduction via photochemical reactions is more

343   rapid than hydrolysis during the daytime (Xu et al., 2001). The COS concentration depends on the light intensity

344   (Ferek and Andreae, 1984). The maximum COS concentration occurred 3 h after the maximal global radiation

345   intensity (COS: 15:00; global radiation intensity: 12:00) due to the balance between COS production and removal (Xu

346   et al., 2001).

347   **4.2 VSCs in the atmosphere**

348   Similar to our results for the VSC mixing ratios in the atmosphere during summer, Kettle et al. (2001) found that the

349   COS mixing ratio in the Atlantic Ocean atmosphere was 552 pptv, while Cooper and Saltzman (1993) measured a

350   DMS mixing ratio of 118 pptv. In addition, the mixing ratios of atmospheric CS_2 in this study were similar to those in

351   a polluted atmosphere (Sandalls and Penkett, 1977) but much higher than those in unpolluted atmospheres, such as

352   over the North Atlantic (Cooper and Saltzman, 1993). This finding indicated that industrial production and human

353   activities significantly affect the mixing ratios of CS_2 in the atmosphere. The mean VSC mixing ratios in the

354   atmosphere during summer in this study were all higher than those in the Changjiang estuary and the adjacent East

355   China Sea (Yu et al., 2022), and the Western Pacific during autumn (Xu et al., 2023).

356   No significant correlation was found between the oceanic VSC concentrations and atmospheric VSC mixing ratios

357   (Table 1). The reason may be that VSCs in the atmosphere were not only derived from sea-to-air diffusion but also

358   from anthropogenic sources, such as the soil, incomplete burning of biomass, and industrial releases (Blake et al.,

359   2004; Chin and Davis, 1993; Whelan et al., 2018). Anthropogenic VSC emissions can be evaluated using isotope

360   measurements (Hattori et al., 2020). However, anthropogenic VSCs emissions were not evaluated in this study, and

361   isotope measurements will be obtained in future studies. The highest mixing ratios of atmospheric COS at station B72

362   and DMS at station B08 in spring coincided with anthropogenic emissions and high DMS concentration in seawater,

363   respectively (Fig. 6). The CS_2 generated by industrial activities may have influenced the atmosphere at station B49,

364   which is near industrial cities, such as Tianjin. Chemical production and pharmaceutical industries are large emitters

365   of CS_2 into the atmosphere (Chin and Davis, 1993). CS_2 is the main precursor of COS in the atmosphere, and

366   atmospheric CS_2 is oxidized to COS by radicals such as OH with a conversion efficiency of 0.81 (Chin and Davis,

367   1995). The significant correlation between atmospheric COS and CS_2 in our study (Table 1) demonstrated this.

368   The 72 h backward trajectories showed that air masses from different sources (land or ocean) and passing through

369   different regions may have affected the atmospheric COS, DMS, and CS_2 mixing ratios. Jiang et al. (2021) stated that

370   different sources of air masses might have affected atmospheric DMS oxidation to MSA. The 72 h backward trajectory

371   over station B49 indicated that the high atmospheric DMS mixing ratio was attributable to human activities. The wind

372   direction is from continental Asia to the Pacific in spring. The backward trajectories of B49, B47, and B08 showed

373   that anthropogenic and oceanic DMS emissions accounted for the atmospheric DMS sources. The wind direction of

374   the air mass from the back trajectories of Miyakojima, Yokohama, and Otaru in Japan in winter (January to March)

375   observed by Hattori et al. (2020) was similar to ours in spring (March to April). Hattori et al. (2020) reported that the

376   anthropogenic COS originated primarily from the Chinese industry and was transported by air to southern Japan. The

377   backward trajectory of H09 showed that the wind direction was from the south of Taiwan Island in summer, and

378   oceanic sources accounted for the atmospheric DMS. The air masses showed that the highest mixing ratios of COS

379   and DMS at station B64 in summer were caused by terrestrial sources from northeast China and oceanic sources in

380   the BS, respectively. The highest CS_2 mixing ratio in summer at station B49 may be due to the air mass transported

381   from the northeast, i.e., industrial cities in China.

382   **4.3 Sea-to-air fluxes of VSCs**

383 The spatial variability in the sea-to-air fluxes was consistent with changes in the wind speed because sea-to-air fluxes

384 depend on the transmission velocities of VSCs in seawater, which are related to the wind speed and viscosity of

385 seawater. Significant correlations between the sea-to-air fluxes of VSCs and the wind speeds confirmed this. In

386 addition, the sea-to-air fluxes of all three VSCs were positive in spring and summer, indicating that the seawater was

387 a source of COS, DMS, and CS_2 to the atmosphere through sea-to-air diffusion. Although our findings agree with

388 those of Chin and Davis (1993) and Yu et al. (2022), who showed that the ocean was a major atmospheric source of

389 COS, they conflict with the results of Weiss et al. (1995) and Zhu et al. (2019), who found significant COS

390 undersaturation in some sea areas. Therefore, the ocean may be a sink of atmospheric COS in some areas or at certain

391 times of the year.

392 The model of Lennartz et al. (2021) was not used to evaluate the global sea-air fluxes of DMS, OCS, CS_2 in this

393 study due to a lack of parameters, i.e., the absorption coefficient of CDOM at 350 nm (a350), global radiation

394 (converted to UV radiation), and sea surface pressure. Therefore, the global sea-air fluxes of DMS were calculated

395 following Hulswar et al. (2022) with minor modifications. The global sea-air fluxes of OCS or CS_2 were evaluated by

396 the mean sea-air fluxes of OCS or CS_2 multiplied by the ocean area and the time. The global sea-air fluxes of DMS,

397 OCS, and CS_2 were 21.3, 2.3, and 2.0 TgS year^{-1}, respectively. The global sea-air flux of DMS was similar to the

398 results of Hulswar et al. (2022) (27.1 TgS year^{-1}). In comparison, the global sea-air fluxes of OCS and CS_2 were 15.9-

399 and 9.9-fold higher than the results of Lennartz et al. (2021). The different calculation method we used may

400 overestimate the global sea-air fluxes of OCS and CS_2. The another reason may be the high sea-air fluxes of OCS or

401 CS_2 in the BS and YS because marginal seas are significantly influenced by anthropogenic emissions (Watts, 2000).

402 The sea-air fluxes of DMS, OCS, and CS_2 in the BS and YS were 28.2, 3.1, and 2.7 GgS year^{-1}, accounting for 0.10%,

403 2.23%, and 1.44% of global sea-air fluxes. The BS and YS comprise 0.13% of the global sea area; therefore, they

404 contribute considerably to global sea-air fluxes.

405 **5 Conclusions**

406 The COS, DMS, and CS_2 distributions in the surface seawater and marine atmosphere of the BS and YS during spring

407 and summer exhibited significant spatial and seasonal variability. First, the COS, DMS, and CS_2 concentrations were

408 higher in summer than in spring. Second, the COS, DMS, and CS_2 concentrations were the highest in the surface

409 seawater and decreased with the depth. The positive correlation between the oceanic COS and DOC concentrations in

410 summer suggested the photochemical production of COS from CDOM. In addition, the atmospheric VSC mixing

411 ratios of the BS and YS exhibited substantial seasonal differences, with higher mixing ratios in summer than in spring.

412 There was a significant correlation between the atmospheric COS and CS_2 mixing ratios, which may verify the COS

413 production from oxidation of CS_2. The backward trajectories showed that the atmospheric mixing ratios of VSCs were

414 affected by anthropogenic and/or oceanic emissions. Finally, the high sea-to-air fluxes of COS, DMS, and CS_2 in the

415 BS and YS indicated that marginal seas are major sources of atmospheric VSCs and may contribute considerably to

416 the global sulfur budget.

426 **References**

427 Andreae, M. O., and Crutzen, P. J.: Atmospheric aerosols: biogeochemical sources and role in atmospheric chemistry,

428   Science, 276 (5315), 1052–1058, https://doi.org/10.1126/science.276.5315.1052, 1997.

429 Aydin, M., Britten, G. L., Montzka, S. A., Buizert, C., Primeau, F. W., Petrenko, V. V., Battle, M. O., Nicewonger,

430   M. R., Patterson, J., Hmiel, B., and Saltzman, E. S.: Anthropogenic impacts on atmospheric carbonyl sulfide since

431   the 19th century inferred from polar firn air and ice core measurements, J. Geophys. Res.-Atmos., 125(16),

432   e2020JD033074, https://doi.org/10.1002/essoar.10503126.1, 2020.

433 Blake, N. J., Streets, D. G., Woo, J.-H., Simpson, I. J., Green, J., Meinardi, S., Kita, K., Atlas, E., Fuelberg, H. E.,

434   Sachse, G., Avery, M. A., Vay, S. A., Talbot, R. W., Dibb, J. E., Bandy, A. R., Thornton, D. C., Rowland, F. S.,

435   and Blake, D. R.: Carbonyl sulfide and carbon disulfide: large-scale distributions over the western Pacific and

436   emissions   from   Asia   during   TRACE-P,   J.   Geophys.   Res.-Atmos.,   109,   D15S05,

437   https://doi.org/10.1029/2003JD004259, 2004.

438   Brown, A. S., van der Veen, A. M. H., Arrhenius, K., Murugan, A., Culleton, L. P., Ziel, P. R., and Li, J.: Sampling

439   of gaseous sulfur-containing compounds at low concentrations with a review of best-practice methods for biogas

440   and natural gas applications, Trac-Trends Anal. Chem., 64, 42–52, https://doi.org/10.1016/j.trac.2014.08.012, 2015.

441   Brühl, C., Lelieveld, J., Crutzen, P. J., and Tost, H.: The role of carbonyl sulphide as a source of stratospheric sulphate

442   aerosol and its impact on climate, Atmos. Chem. Phys., 12(3), 1239–1253, http://dx.doi.org/10.5194/acp-12-1239-

443   2012, 2012.

444   Campbell, J. E., Carmichael, G. R., Chai T., Mena-Carrasco, M., Tang, Y., Blake, D. R., Blake, N. J., Vay, S. A.,

445   Collatz, G. J., Baker, I., Berry, J. A., Montzka, S. A., Sweeney, C., Schnoor, J. L., and Stanier, C. O.: Photosynthetic

446   control of atmospheric carbonyl sulfide during the growing season, Science, 322, 1085–1088,

447   https://doi.org/10.1126/science.1164015, 2008.

448   Campbell, J. E., Whelan, M. E., Seibt U., Smith S. J., Berry, J. A., and Hilton, T. W.: Atmospheric carbonyl sulfide

449   sources from anthropogenic activity: Implications for carbon cycle constraints, Geophys. Res. Lett., 42, 3004–3010,

450   https://doi.org/10.1002/2015GL063445, 2015.

451   Charlson, R. J., Lovelock, J. E., Andreae, M. O., and Warren, S. G.: Oceanic phytoplankton, atmospheric sulphur,

452   cloud albedo and climate, Nature, 326, 655–661, https://doi.org/10.1038/326655a0, 1987.

453   Chen C.-T. A.: Chemical and physical fronts in the Bohai, Yellow and East China seas, J. Mar. Syst., 78(3), 394–410,

454   https://doi.org/10.1016/j.jmarsys.2008.11.016, 2009.

455   Chen, Y., Wang, P., Shi, D., Ji, C.-X., Chen, R., Gao, X.-C., and Yang, G.-P.: Distribution and bioavailability of

456   dissolved and particulate organic matter in different water masses of the Southern Yellow Sea and East China Sea,

457   J. Marine Syst., 222, 103596, https://doi.org/10.1016/j.jmarsys.2021.103596, 2021.

458   Chin, M., and Davis, D. D.: Global sources and sinks of OCS and CS_2 and their distributions, Global Biogeochem.

459   Cy., 7(2), 321–337, https://doi.org/10.1029/93GB00568, 1993.

460   Chin, M., and Davis, D. D.: A reanalysis of carbonyl sulfide as a source of stratospheric background sulfur aerosol, J.

461   Geophys. Res.-Atmos., 100(D5), 8993–9005, https://doi.org/10.1029/95JD00275, 1995.

462 Chu, C., Erickson, P. R., Lundeen, R. A., Stamatelatos, D., Alaimo, P. J., Latch D. E., and McNeill, K.: Photochemical

463   and nonphotochemical transformations of cysteine with dissolved organic matter, Environ. Sci. Technol., 50, 6363–

464   6373, https://doi.org/10.1021/acs.est.6b01291, 2016.

465 Cline, J. D., and Bates, T. S.: Dimethyl sulfide in the Equatorial Pacific Ocean: a natural source of sulfur to the

466   atmosphere, Geophys. Res. Lett., 10(10), 949–952, https://doi.org/10.1029/GL010i010p00949, 1983.

467 Cooper, D. J., and Saltzman, E. S.: Measurements of atmospheric dimethylsulfide, hydrogen sulfide, and carbon

468   disulfide   during   GTE/CITE   3,   J.   Geophys.   Res.-Atmos.,   98(D12),   23397–23409,

469   https://doi.org/10.1029/92JD00218, 1993.

470 Crutzen, P. J.: The possible importance of CSO for the sulfate layer of the stratosphere, Geophys. Res. Lett., 3(2), 73–

471   76, https://doi.org/10.1029/GL003i002p00073, 1976.

472 Curson, A. R. J., Liu, J., Bermejo Mart ńez, A., Green, R. T., Chan, Y., Carri ón, O., Williams, B. T., Zhang, S.-H.,

473   Yang, G.-P., Bulman Page, P. C., Zhang, X.-H., and Todd, J. D.: Dimethylsulfoniopropionate biosynthesis in marine

474   bacteria   and   identification   of   the   key   gene   in   this   process,   Nat.   Microbiol.,   2:   17009,

475   https://doi.org/10.1038/nmicrobiol.2017.9, 2017.

476 Dacey, J. W. H., Wakeham, S. G., and Howes, B. L.: Henry's law constants for dimethylsulfide in freshwater and

477   seawater, Geophys. Res. Lett., 11, 991–994, https://doi.org/10.1029/GL011i010p00991, 1984.

478 De Bruyn, W. J., Swartz, E., Hu, J. H., Shorter, J. A., Davidovits, P., Worsnop, D. R., Zahniser, M. S., and Kolb, C.

479   E.: Henry's law solubilities and Šetchenow coefficients for biogenic reduced sulfur species obtained from gas-liquid

480   uptake measurements, J. Geophys. Res.-Atmos., 100, 7245–7251, https://doi.org/10.1029/95JD00217, 1995.

481 Du, Q., Mu, Y., Zhang, C., Liu, J., Zhang, Y., and Liu, C.: Photochemical production of carbonyl sulfide, carbon

482   disulfide   and   dimethyl   sulfide   in   a   lake   water,   J.   Environ.   Sci.,   51,   146–156,

483   https://doi.org/10.1016/j.jes.2016.08.006, 2017.

484 Ferek, R. J., and Andreae, M. O.: Photochemical production of carbonyl sulphide in marine surface waters. Nature,

485   307, 148–150, https://doi.org/10.1038/307148a0, 1984.

486 Ferek, R. J., and Andreae, M. O.: The supersaturation of carbonyl sulfide in surface waters of the Pacific Ocean off

487   Peru, Geophys. Res. Lett., 10(5), 393–396, https://doi.org/10.1029/GL010I005P00393, 1983.

488   Flöck, O. R., Andreae, M. O., and Dräger, M.: Environmentally relevant precursors of carbonyl sulfide in aquatic

489   systems, Mar. Chem., 59(1-2), 71–85, https://doi.org/10.1016/S0304-4203(97)00012-1, 1997.

490   Guéguen, C., Guo, L., and Tanaka, N.: Distributions and characteristics of colored dissolved organic matter in the

491   Western Arctic Ocean, Cont. Shelf Res., 25, 1195–1207, https://doi.org/10.1016/j.csr.2005.01.005, 2005.

492   Hattori, S., Kamezaki, K., and Yoshida, N.: Constraining the atmospheric OCS budget from sulfur isotopes, Proc.

493   Natl. Acad. Sci. U.S.A., 117(34), 20447–20452, https://doi.org/10.1073/pnas.2007260117, 2020.

494   Hobe, M. V., Cutter, G. A., Kettle, A. J., and Andreae, M. O.: Dark production: a significant source of oceanic COS,

495   J. Geophys. Res.-Oceans., 106(C12), 31217–31226, https://doi.org/10.1029/2000JC000567, 2001.

496   Hulswar, S., Simó, R., Galí, M., Bell, T. G., Lana, A., Inamdar, S., Halloran, P. R., Manville, G., and Mahajan, A. S.:

497   Third revision of the global surface seawater dimethyl sulfide climatology (DMS-Rev3), Earth Syst. Sci. Data, 14,

498   2963–2987, https://doi.org/10.5194/essd-14-2963-2022, 2022.

499   Inomata, Y., Hayashi, M., Osada, K., and Iwasaka, Y.: Spatial distributions of volatile sulfur compounds in surface

500   seawater and overlying atmosphere in the northwestern Pacific Ocean, eastern Indian Ocean, and Southern Ocean,

501   Global Biogeochem. Cy., 20(2), GB2022, https://doi.org/10.1029/2005GB002518, 2006.

502   Jiang, B., Xie, Z., Qiu, Y., Wang, L., Yue, F., Kang, H., Yu, X., and Wu, X.: Modification of the conversion of

503   dimethylsulfide to methanesulfonic acid by anthropogenic pollution as revealed by long-term observations, ACS

504   Earth Space Chem., 5, 2839−2845, https://doi.org/10.1021/acsearthspacechem.1c00222, 2021.

505   Keller, M. D., Bellows, W. K., and Guillard, R. R. L.: Dimethyl sulfide production in marine phytoplankton, in:

506   Biogenic sulfur in the environment, edited by: Millero, F. J., Hershey, J. P., Saltzman, E. S., and Cooper, W. J.,

507   American Chemical Society, Washington, DC, 167–182, http://dx.doi.org/10.1021/bk-1989-0393.ch011, 1989.

508   Kettle, A. J., Kuhn, U., von Hobe, M., Kesselmeier, J., and Andreae, M. O.: Global budget of atmospheric carbonyl

509   sulfide: temporal and spatial variations of the dominant sources and sinks, J. Geophys. Res., 107(D22), 4658,

510   https://doi.org/10.1029/2002JD002187, 2002.

511   Kettle, A. J., Rhee, T. S., von Hobe, M., Poulton, A., Aiken, J., and Andreae, M. O.: Assessing the flux of different

512   volatile sulfur gases from the ocean to the atmosphere, J. Geophys. Res.-Atmos., 106(D11), 12193–12209,

513   https://doi.org/10.1029/2000JD900630, 2001.

Kim, K.-H., and Andreae, M. O.: Carbon disulfide in estuarine, coastal and oceanic environments, Mar. Chem., 40, 179–197, https://doi.org/10.1016/0304-4203(92)90022-3, 1992.

Kurian S, Chndrasekhararao A. V., Vidya P. J., Shenoy D. M., Gauns M., Uskaikar, H., and Aparna, S. G.: Role of oceanic fronts in enhancing phytoplankton biomass in the eastern Arabian Sea during an oligotrophic period, Mar. Environ. Res., 160, 105023, https://doi.org/10.1016/j.marenvres.2020.105023, 2020.

Lennartz, S. T., Gauss, M., von Hobe, M., and Marandino, C. A.: Monthly resolved modelled oceanic emissions of carbonyl sulphide and carbon disulphide for the period 2000–2019, Earth Syst. Sci. Data, 13, 2095–2110, https://doi.org/10.5194/essd-13-2095-2021, 2021.

Lennartz, S. T., Marandino, C. A., von Hobe, M., Andreae, M. O., Aranami, K., Atlas, E., Berkelhammer, M., Bingemer, H., Booge, D., Cutter, G., Cortes, P., Kremser, S., Law, C. S., Marriner, A., Simó, R., Quack, B., Uher, G., Xie, H., and Xu, X.: Marine carbonyl sulfide (OCS) and carbon disulfide (CS_2): a compilation of measurements in seawater and the marine boundary layer, Earth Syst. Sci. Data, 12, 591–609, https://doi.org/10.5194/essd-12-591-2020, 2020.

Lennartz, S. T., Marandino, C. A., von Hobe, M., Cortes, P., Quack, B., Simo, R., Booge, D., Pozzer, A., Steinhoff, T., Arevalo-Martinez, D. L., Kloss, C., Bracher, A., Röttgers, R., Atlas, E., and Krüger, K.: Direct oceanic emissions unlikely to account for the missing source of atmospheric carbonyl sulfide, Atmos. Chem. Phys., 17, 385–402, https://doi.org/10.5194/acp-17-385-2017, 2017.

Li, J.-L., Zhai, X., and Du, L.: Effect of nitrate on the photochemical production of carbonyl sulfide from surface seawater, Geophys. Res. Lett., 49, e2021GL097051, https://doi.org/10.1029/2021GL097051, 2022.

Liss, P. S., and Slater, P. G.: Flux of gases across the air-sea interface, Nature, 247(5438), 181–184, https://doi.org/10.1038/247181a0, 1974.

Maignan, F., Abadie, C., Remaud, M., Kooijmans, L. M. J., Kohonen, K.-M., Commane, R., Wehr, R., Campbell, J. E., Belviso, S., Montzka, S. A., Raoult, N., Seibt, U., Shiga, Y. P., Vuichard, N., Whelan, M. E., and Peylin, P.: Carbonyl sulfide: comparing a mechanistic representation of the vegetation uptake in a land surface model and the leaf relative uptake approach, Biogeosciences, 18, 2917–2955, https://doi.org/10.5194/bg-18-2917-2021, 2021.

Modiri Gharehveran, M., Hain E, Blaney L, and Shah, A. D.: Influence of dissolved organic matter on carbonyl sulfide and carbon disulfide formation from cysteine during sunlight photolysis, Environ. Sci.: Processes Impacts, 22,

541   1852–1864, https://doi.org/10.1039/D0EM00219D, 2020.

542   Modiri Gharehveran, M., and Shah, A. D.: Influence of dissolved organic matter on carbonyl sulfide and carbon

543   disulfide formation from dimethyl sulfide during sunlight photolysis, Water Environ. Res., 93, 2982–2997,

544   https://doi.org/10.1002/wer.1650, 2021.

545   Naik, B. R., Gauns, M., Bepari, K., Uskaikar, H., and Shenoy, D. M.: Variation in phytoplankton community and its

546   implication to dimethylsulphide production at a coastal station off Goa, India, Mar. Environ. Res., 157, 104926,

547   https://doi.org/10.1016/j.marenvres.2020.104926, 2020.

548   Nightingale, P. D., Malin, G., Law, C. S., Watson, A. J., Liss, P. S., Liddicoat, M. I., Boutin, J., and Upstill-Goddard,

549   R. C.: In situ evaluation of air-sea gas exchange parameterizations using novel conservative and volatile tracers,

550   Global Biogeochem. Cy., 14(1), 373–387, https://doi.org/10.1029/1999GB900091, 2000.

551   O'Brien, J., McParland, E. L., Bramucci, A. R., Ostrowski, M., Siboni, N., Ingleton, T., Brown, M. V., Levine, N. M.,

552   Laverock, B., Petrou, K., and Seymour, J.: The microbiological drivers of temporally dynamic

553   dimethylsulfoniopropionate cycling processes in Australian coastal shelf waters, Front. Microbiol., 13, 894026,

554   https://doi.org/10.3389/fmicb.2022.894026, 2022.

555   Parsons, T. R., Maita, Y., and Lalli, C. M.: A manual of chemical and biological methods for seawater analysis, in

556   Fluorometric determination of chlorophylls, edited by: Parsons, T. R., Maita, Y., and Lalli, C. M., Great Britain,

557   CA: Pergamon Press, 107–109, 1984.

558   Reisch, C. R., Stoudemayer, M. J., Varaljay, V. A., Amster, I. J., Moran, M. A., and Whitman, W. B.: Novel pathway

559   for assimilation of dimethylsulphoniopropionate widespread in marine bacteria, Nature, 473(7346), 208–211,

560   https://doi.org/10.1038/nature10078, 2011.

561   Remaud, M., Chevallier, F., Maignan, F., Belviso, S., Berchet, A., Parouffe, A., Abadie, C., Bacour, C., Lennartz, S.,

562   and Peylin, P.: Plant gross primary production, plant respiration and carbonyl sulfide emissions over the globe

563   inferred by atmospheric inverse modelling, Atmos. Chem. Phys., 22(4), 2525–2552, https://doi.org/10.5194/acp-

564   22-2525-2022, 2022.

565   Sandalls, F. J., and Penkett, S. A.: Measurements of carbonyl sulphide and carbon disulphide in the atmosphere, Atmos.

566   Environ., 11(2), 197–199, https://doi.org/10.1016/0004-6981(77)90227-X, 1977.

567   Sander, R.: Compilation of Henry's law constants (version 4.0) for water as solvent, Atmos. Chem. Phys., 15, 4399–

568   4981, https://doi.org/10.5194/acp-15-4399-2015, 2015.

569   Schäfer, H., Myronova, N., and Boden, R.: Microbial degradation of dimethylsulphide and related C_1-sulphur

570   compounds: organisms and pathways controlling fluxes of sulphur in the biosphere, J. Exp. Bot., 61(2), 315–334,

571   https://doi.org/10.1093/jxb/erp355, 2010.

572   Schlitzer, R.: Ocean Data View, odv.awi.de, 2023.

573   Sciare, J., Mihalopoulos, N., and Nguyen, B. C.: Spatial and temporal variability of dissolved sulfur compounds in

574   European estuaries, Biogeochemistry, 59(1–2), 121–141, http://dx.doi.org/10.1023/A:1015539725017, 2002.

575   Simó, R., Grimalt, J. O., and Albaigés, J.: Dissolved dimethylsulphide, dimethylsulphoniopropionate and

576   dimethylsulphoxide in western Mediterranean waters, Deep-Sea Res. Pt II, 44(3-4), 929–950,

577   https://doi.org/10.1016/S0967-0645(96)00099-9, 1997.

578   Staubes, R., and Georgii, H.-W.: Biogenic sulfur compounds in seawater and the atmosphere of the Antarctic region,

579   Tellus B, 45(2), 127–137, https://doi.org/10.3402/tellusb.v45i2.15587, 1993.

580   Tian, X., Hu, M., and Ma, Q.: Determination of volatile sulfur compounds in the atmosphere and surface seawater in

581   Qingdao, Acta Scien. Circum., 25(1), 30–33, (in Chinese with English abstract),

582   https://doi.org/10.13671/j.hjkxxb.2005.01.005, 2005.

583   Uher, G., and Andreae, M. O.: Photochemical production of carbonyl sulfide in North Sea water: a process study,

584   Limnol. Oceanogr., 42(3), 432–442, https://doi.org/10.4319/lo.1997.42.3.0432, 1997.

585   Ulshöfer, V. S., Flöck, O. R., Uher, G., and Andreae, M. O.: Photochemical production and air-sea exchange of

586   carbonyl sulfide in the eastern Mediterranean Sea, Mar. Chem., 53(53), 25–39, https://doi.org/10.1016/0304-

587   4203(96)00010-2, 1996.

588   Ulshöfer, V. S., Uher, G., and Andreae, M. O.: Evidence for a winter sink of atmospheric carbonyl sulfide in the

589   northeast Atlantic Ocean, Geophys. Res. Lett., 22(19), 2601–2604, https://doi.org/10.1029/95GL02656, 1995.

590   Wang, J., Chu, Y.-X., Tian, G., and He, R.: Estimation of sulfur fate and contribution to VSC emissions from lakes

591   during algae decay, Sci. Total Environ., 856, 159193, http://dx.doi.org/10.1016/j.scitotenv.2022.159193, 2023.

592   Watts, S. F.: The mass budgets of carbonyl sulfide, dimethyl sulfide, carbon disulfide and hydrogen sulfide, Atmos.

593   Environ., 34, pp. 761-779, https://doi.org/10.1016/S1352-2310(99)00342-8, 2000.

594 Weiss, P. S., Johnson, J. E., Gammon, R. H., and Bates, T. S.: Reevaluation of the open ocean source of carbonyl

595   sulfide to the atmosphere, J. Geophys. Res.-Atmos., 100(D11), 23083–23092, https://doi.org/10.1029/95JD01926,

596   1995.

597 Whelan, M. E., Lennartz, S. T., Gimeno, T. E., Wehr, R., Wohlfahrt, G., Wang, Y., Kooijmans, L. M. J., Hilton, T.

598   W., Belviso, S., Peylin, P., Commane, R., Sun, W., Chen, H., Kuai, L., Mammarella, I., Maseyk, K., Berkelhammer,

599   M., Li, K.-F., Yakir, D., Zumkehr, A., Katayama, Y., Ogée, J., Spielmann, F. M., Kitz, F., Rastogi, B., Kesselmeier,

600   J., Marshall, J., Erkkilä, K.-M., Wingate, L., Meredith, L. K., He, W., Bunk, R., Launois, T., Vesala, T., Schmidt,

601   J. A., Fichot, C. G., Seibt, U., Saleska, S., Saltzman, E. S., Montzka, S. A., Berry, J. A., and Campbell, J. E.:

602   Reviews and syntheses: carbonyl sulfide as a multi-scale tracer for carbon and water cycles, Biogeosciences, 15,

603   3625–3657, https://doi.org/10.5194/bg-15-3625-2018, 2018.

604 Xie, H., Moore, R. M., and Miller, W. L.: Photochemical production of carbon disulphide in seawater, J. Geophys.

605   Res.-Oceans, 103(C3), 5635–5644, https://doi.org/10.1029/97JC02885, 1998.

606 Xu, F., Zhang, H.-H., Yan, S.-B., Sun, M.-X., Wu, J.-W., and Yang, G.-P.: Biogeochemical controls on climatically

607   active gases and atmospheric sulfate aerosols in the western Pacific, Environ. Res., 220, 115211,

608   https://doi.org/10.1016/j.envres.2023.115211, 2023.

609 Xu, X., Bingemer, H. G., Georgii, H.-W., Schmidt, U., and Bartell, U.: Measurements of carbonyl sulfide (COS) in

610   surface seawater and marine air, and estimates of the air-sea flux from observations during two Atlantic cruises, J.

611   Geophys. Res.-Atmos., 106(D4), 3491–3502, https://doi.org/10.1029/2000JD900571, 2001.

612 Yang, G.-P., Jing, W.-W., Kang, Z.-Q., Zhang, H.-H., and Song, G.-S.: Spatial variations of dimethylsulfide and

613   dimethylsulfoniopropionate in the surface microlayer and in the subsurface waters of the South China Sea during

614   springtime, Mar. Environ. Res., 65, 85–97, https://doi.org/10.1016/j.marenvres.2007.09.002, 2008.

615 Yang, G.-P., Song, Y.-Z., Zhang, H.-H., Li, C.-X., and Wu, G.-W.: Seasonal variation and biogeochemical cycling of

616   dimethylsulfide (DMS) and dimethylsulfoniopropionate (DMSP) in the Yellow Sea and Bohai Sea, J. Geophys.

617   Res.-Oceans, 119(12), 8897–8915, https://doi.org/10.1002/2014JC010373, 2014.

618 Yang, G.-P., Zhang, S.-H., Zhang, H.-H., Yang, J., and Liu, C.-Y.: Distribution of biogenic sulfur in the Bohai Sea

619   and northern Yellow Sea and its contribution to atmospheric sulfate aerosol in the late fall, Mar. Chem., 169, 23–

620   32, https://doi.org/10.1016/j.marchem.2014.12.008, 2015.

621 Yu, J., Zhang, S.-H., Tian, J.-Y., Zhang, Z.-Y., Zhao, L.-J., Xu, R., Yang, G.-P., Lai, J.-G., Wang, X.-D.: Distribution

622 and dimethylsulfoniopropionate degradation of dimethylsulfoniopropionate-consuming bacteria in the Yellow Sea

623 and East China Sea, J. Geophys. Res.-Oceans, 126, e2021JC017679, https://doi.org/10.1029/2021JC017679, 2021.

624 Yu, J., Sun, M.-X., and Yang, G.-P.: Occurrence and emissions of volatile sulfur compounds in the Changjiang estuary

625 and the adjacent East China Sea, Mar. Chem., 238, 104062, https://doi.org/10.1016/j.marchem.2021.104062, 2022.

626 Yu, J., Wang, S., Lai, J.-G., Tian, J.-Y., Zhang, H.-Q., Yang, G.-P., and Chen, R.: The effect of zooplankton on the

627 distributions of dimethyl sulfide and dimethylsulfoniopropionate in the Bohai and Yellow Seas, J. Geophys. Res.-

628 Oceans, 128, e2022JC019030, https://doi.org/10.1029/2022JC019030, 2023.

629 Zepp, R. G., and Andreae, M. O.: Factors affecting the photochemical production of carbonyl sulfide in seawater,

630 Geophys. Res. Lett., 21(25), 2813–2816, https://doi.org/10.1029/94GL03083, 1994.

631 Zhang, Y., Tan, D.-D., He, Z., Yu, J., Yang, G.-P.: Dimethylated sulfur, methane and aerobic methane production in

632 the Yellow Sea and Bohai Sea, J. Geophys. Res.-Oceans, 128, e2023JC019736,

633 https://doi.org/10.1029/2023JC019736, 2023.

634 Zhang, S.-H., Yang, G.-P., Zhang, H.-H., and Yang, J.: Spatial variation of biogenic sulfur in the south Yellow Sea

635 and the East China Sea during summer and its contribution to atmospheric sulfate aerosol, Sci. Total Environ., 488-

636 489, 157–167, https://doi.org/10.1016/j.scitotenv.2014.04.074, 2014.

637 Zhao, Y., Schlundt, C., Booge, D., and Bange, H. W.: A decade of dimethyl sulfide (DMS),

638 dimethylsulfoniopropionate (DMSP) and dimethyl sulfoxide (DMSO) measurements in the southwestern Baltic Sea,

639 Biogeosciences, 18, 2161–2179, https://doi.org/10.5194/bg-18-2161-2021, 2021.

640 Zhu, R., Yang, G.-P., and Zhang, H.-H.: Temporal and spatial distributions of carbonyl sulfide, dimethyl sulfide, and

641 carbon disulfide in seawater and marine atmosphere of the Changjiang Estuary and its adjacent East China Sea,

642 Limnol. Oceanogr., 64, 632–649, https://doi.org/10.1002/lno.11065, 2019.

643 Zhu, R., Zhang, H.-H., and Yang, G.-P.: Determination of volatile sulfur compounds in seawater and atmosphere,

644 Chin. J. Anal. Chem., 45(10), 1504–1510, (in Chinese with English abstract), https://doi.org/10.11895/j.issn.0253-

645 3820.170291, 2017.

646 Zumkehr, A., Hilton, T. W., Whelan, M., Smith, S., Kuai, L., Worden, J., and Campbell, J. E.: Global gridded

647   anthropogenic emissions inventory of carbonyl sulfide, Atmos. Environ., 183, 11–19,

648   https://doi.org/10.1016/j.atmosenv.2018.03.063, 2018.

649

Figure captions

651 **Fig. 1.** Sampling stations in the Yellow Sea and Bohai Sea during (a) spring and (b) summer (▲ indicates stations

652 where atmospheric samples were collected). Yellow Sea Cold Water Mass: YSCWM. The maps were plotted with

653 Ocean Data View (ODV software) (Schlitzer, 2023).

654 **Fig. 2.** Spatial distributions of temperature, salinity, Chl *a*, COS, DMS, CS_2, and DOC in the surface water of the BS

655 and YS in spring.

656 **Fig. 3.** Spatial distributions of temperature, salinity, Chl *a*, COS, DMS, CS_2, and DOC in the surface water of the BS

657 and YS in summer.

658 **Fig. 4.** Depth distributions of temperature, salinity, Chl *a*, COS, DMS, and CS_2 in seawater in spring.

659 **Fig. 5.** Depth distributions of temperature, salinity, Chl *a*, COS, DMS, and CS_2 in seawater in summer.

660 **Fig. 6.** Spatial distributions of COS, DMS, and CS_2 in the atmosphere over the BS and YS in (a)-(c) spring and (d)-(f)

661 summer. (Unit: pptv)

662 **Fig. 7.** Variations in sea-to-air fluxes of VSCs, VSCs concentrations in seawater, and wind speeds in the BS and YS

663 in spring 2018.

664 **Fig. 8.** Variations in sea-to-air fluxes of VSCs, VSCs concentrations in seawater, and wind speeds in the BS and YS

665 in summer 2018.
666
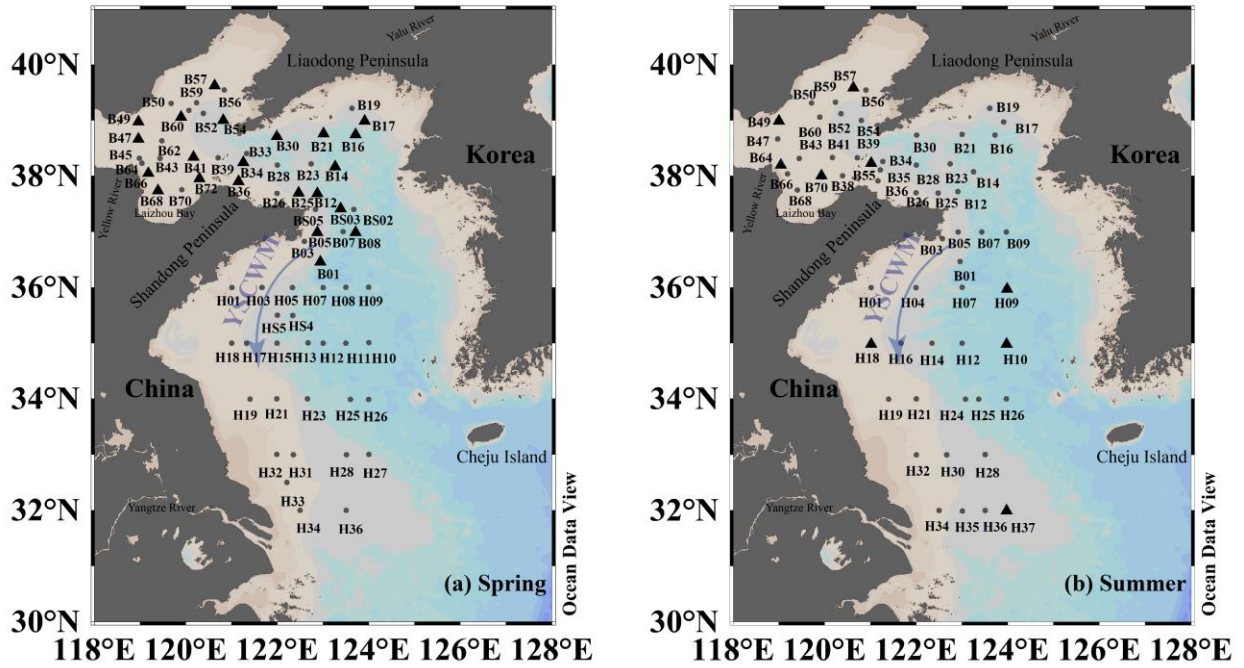
667

Fig. 1. Sampling stations in the Yellow Sea and Bohai Sea during (a) spring and (b) summer (▲ indicates stations where atmospheric samples were collected). Yellow Sea Cold Water Mass: YSCWM. The maps were plotted with Ocean Data View (ODV software) (Schlitzer, 2023).
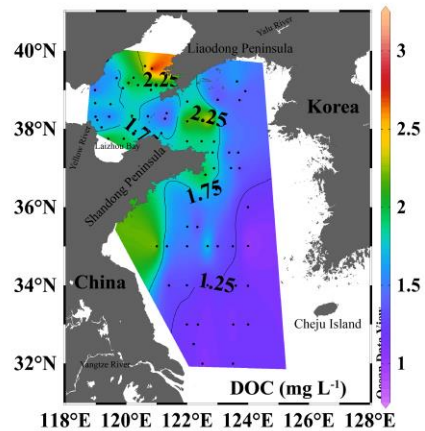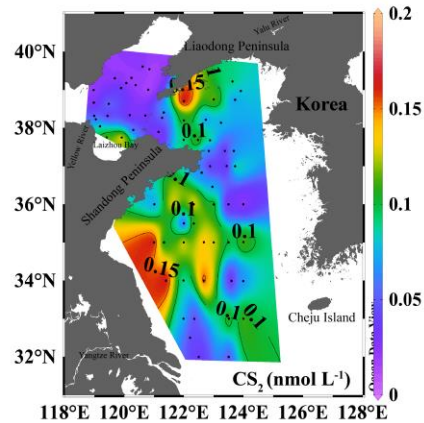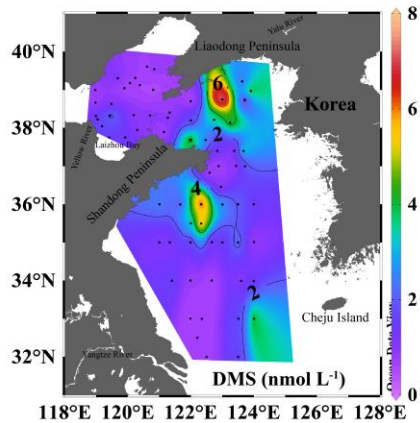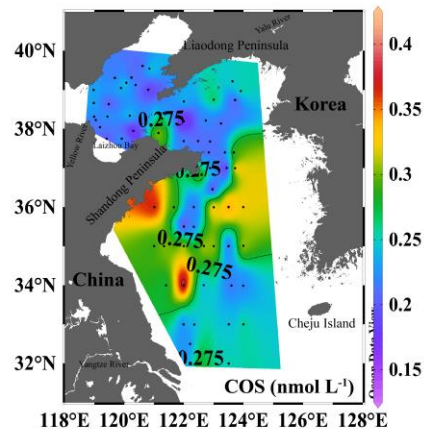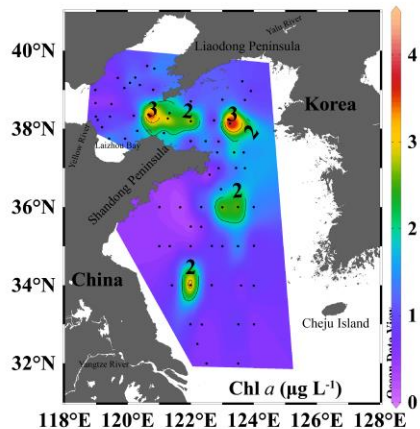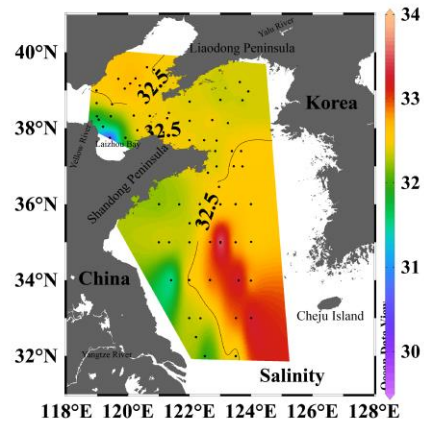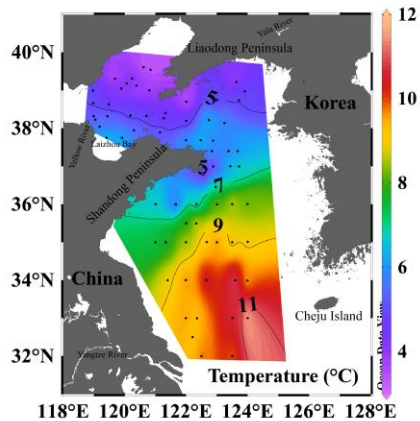
674   **Fig. 2.** Spatial distributions of temperature, salinity, Chl a, COS, DMS, CS$_2$, and DOC in the surface water of the BS

675   and YS in spring.
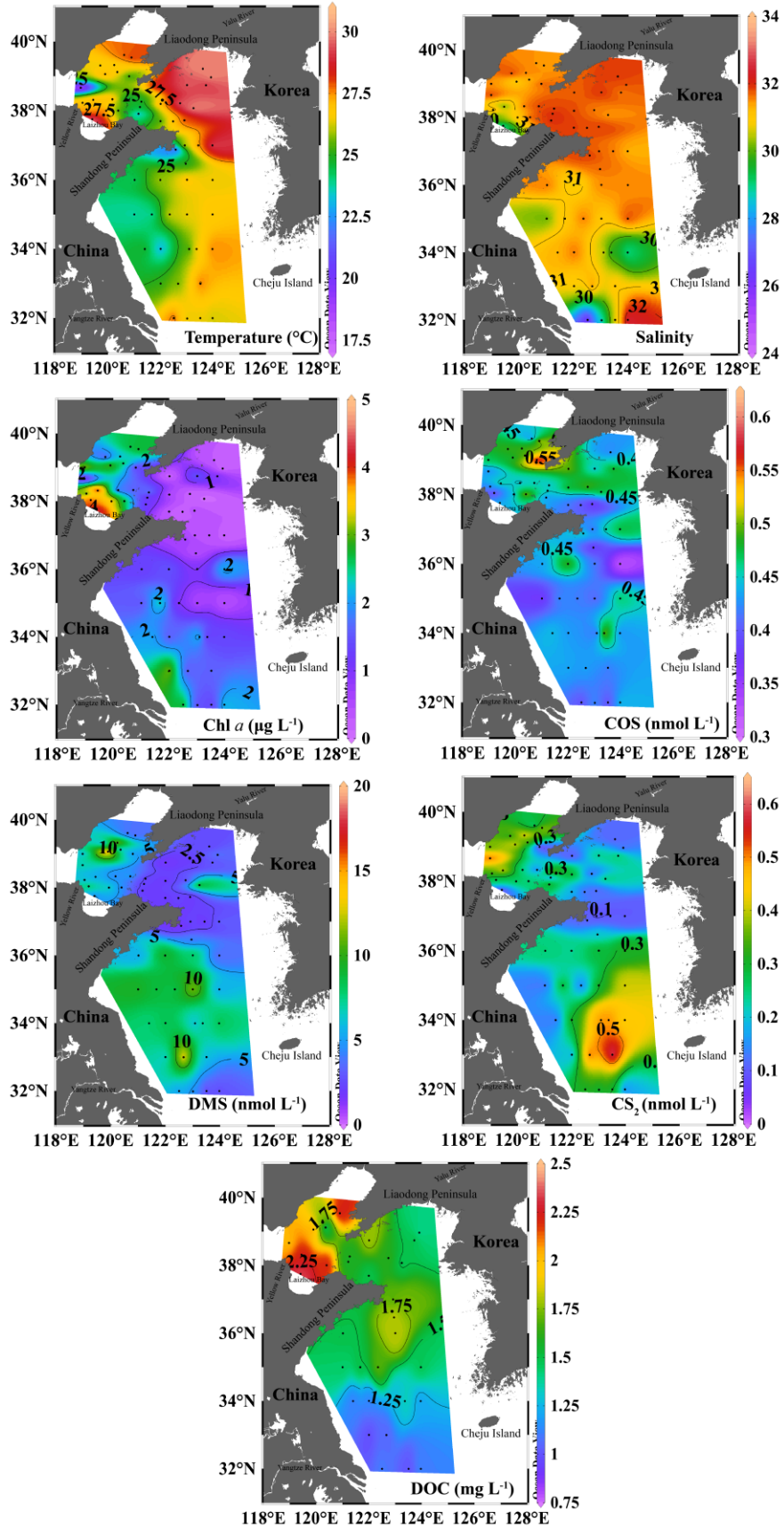
677   **Fig. 3.** Spatial distributions of temperature, salinity, Chl *a*, COS, DMS, CS$_2$, and DOC in the surface water of the BS

678   and YS in summer.
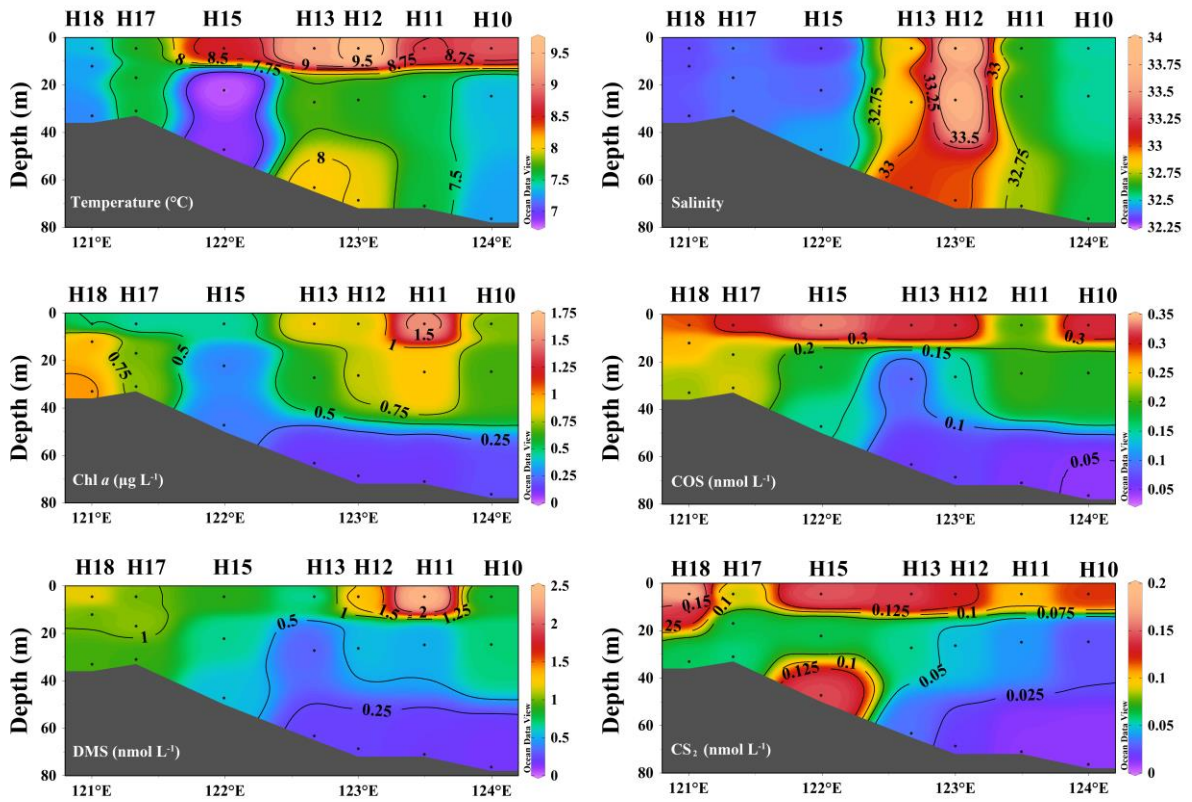
679
680
681   **Fig. 4.** Depth distributions of temperature, salinity, Chl *a*, COS, DMS, and CS$_2$ in seawater in spring.
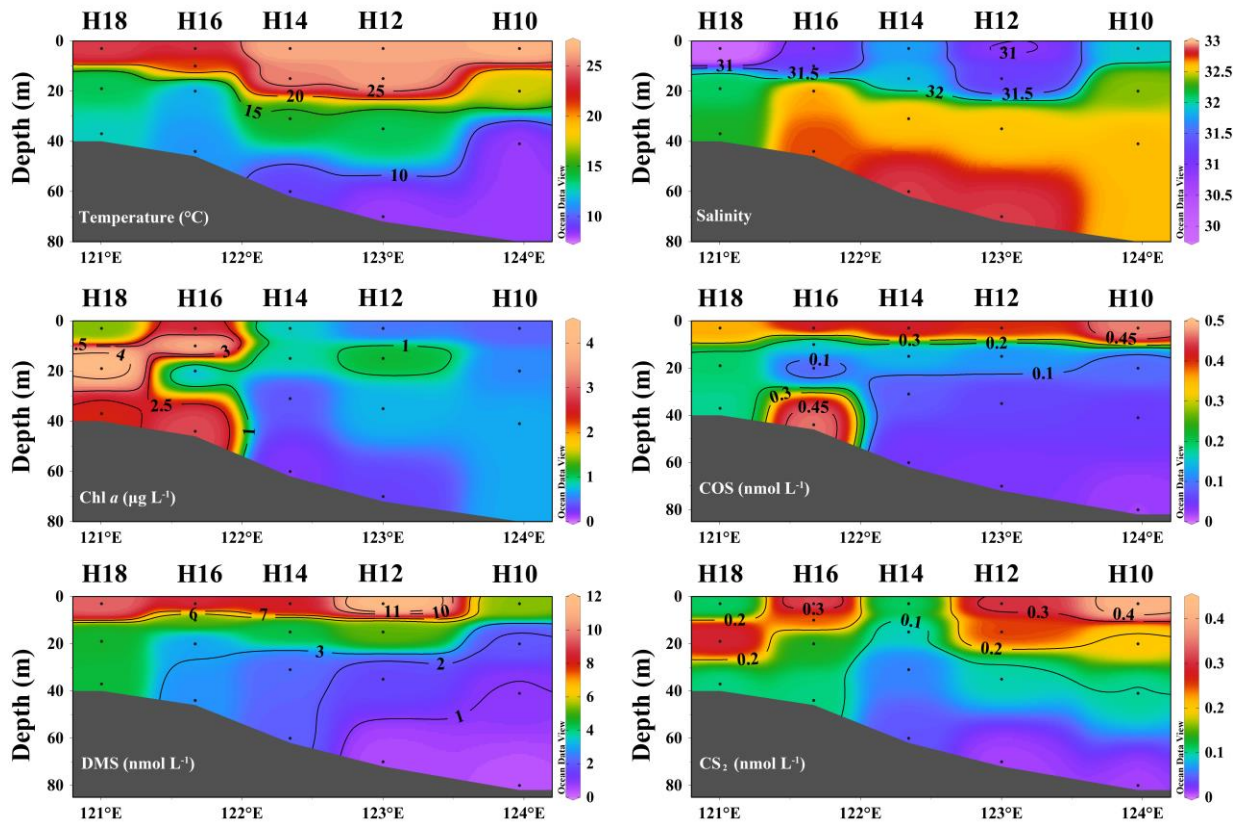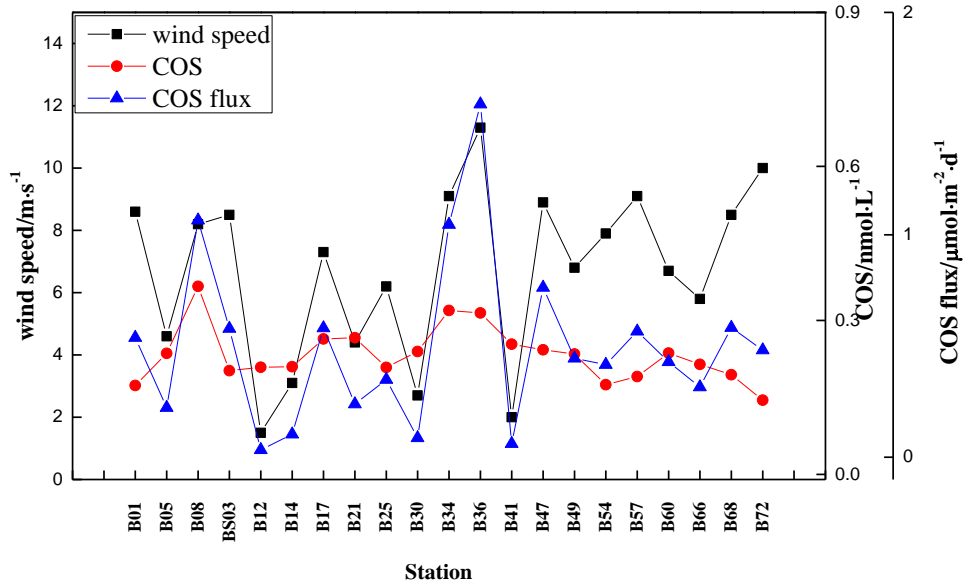
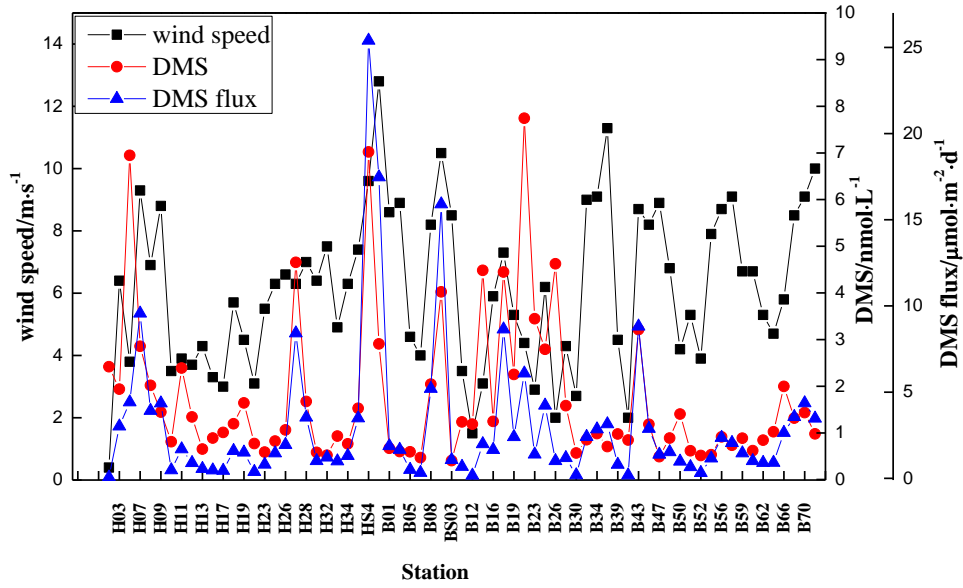**Fig. 5.** Depth distributions of temperature, salinity, Chl *a*, COS, DMS, and CS$_2$ in seawater in summer.
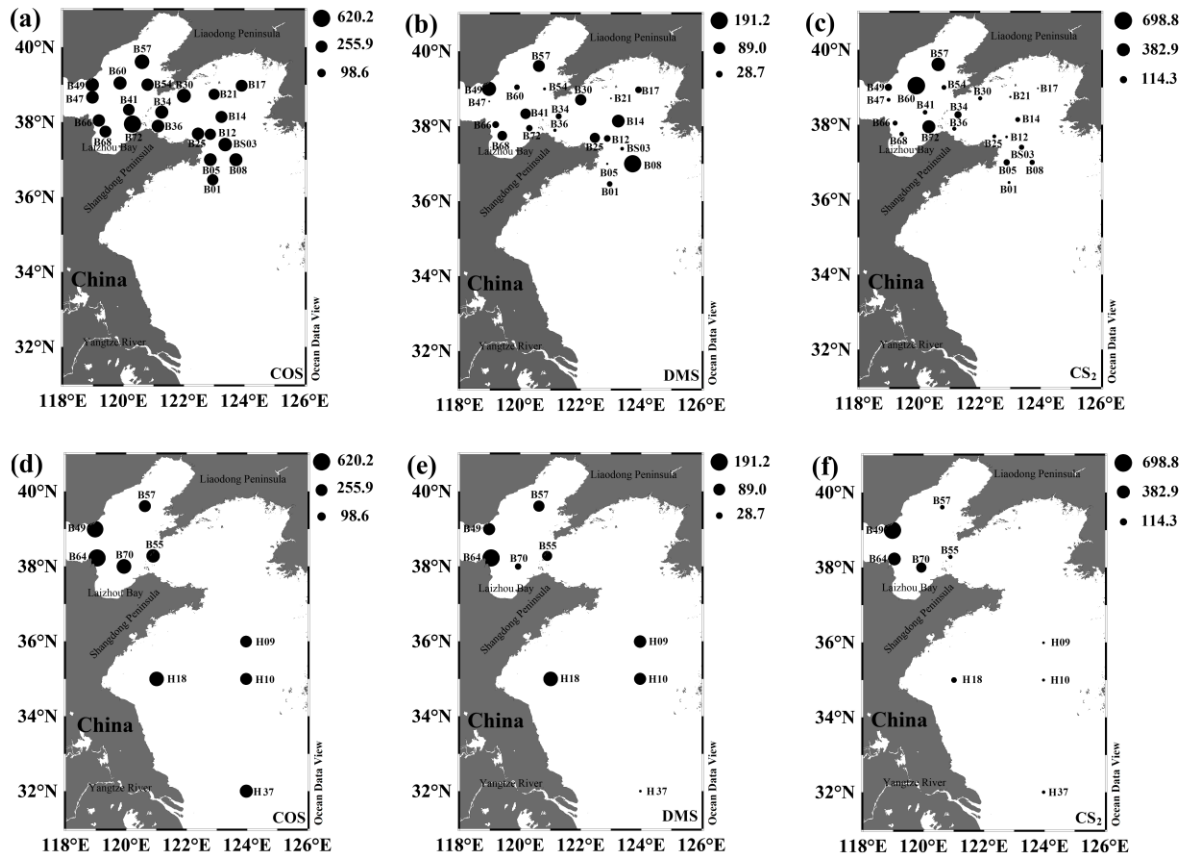
Fig. 6. Spatial distributions of COS, DMS, and CS$_2$ in the atmosphere over the BS and YS in (a)-(c) spring and (d)-(f) summer. (Unit: pptv)
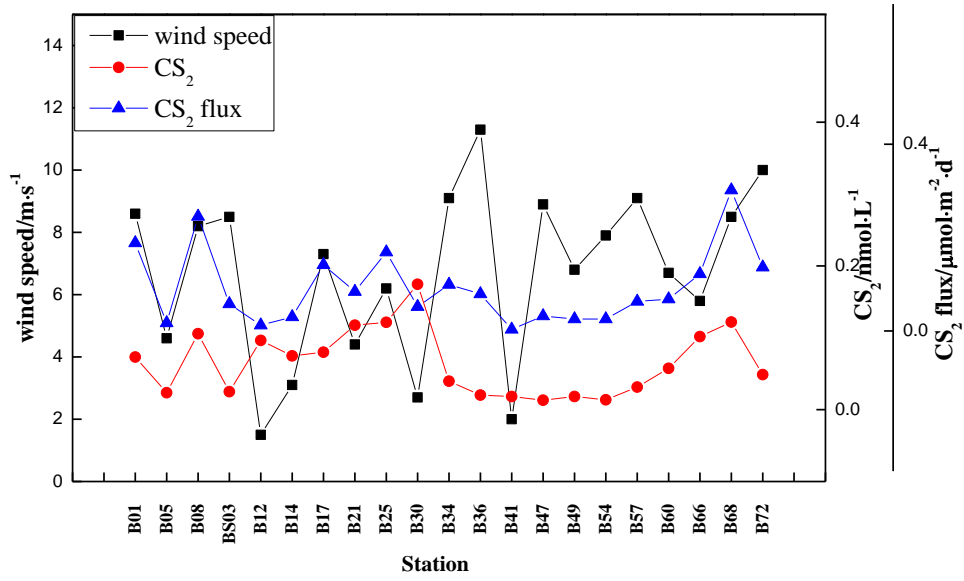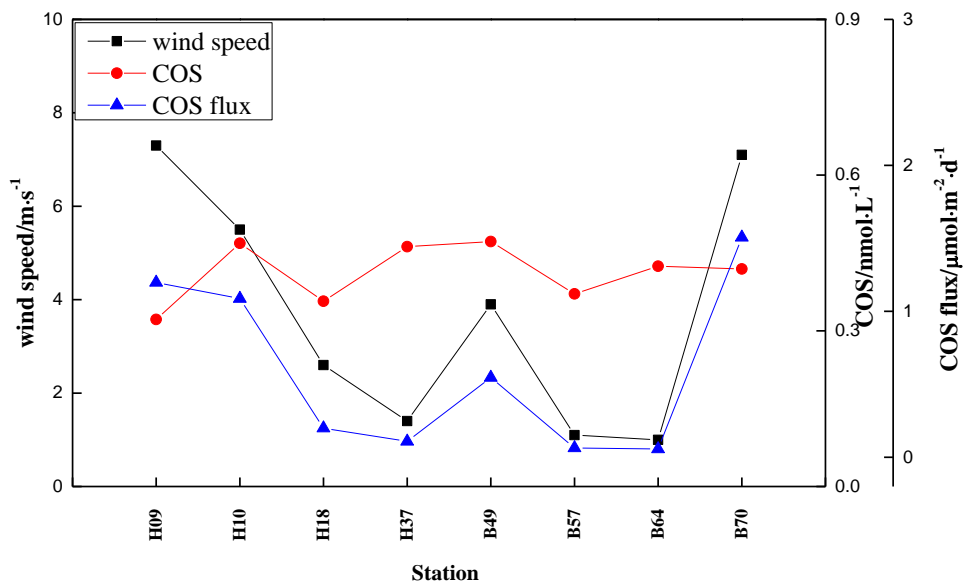
688

689
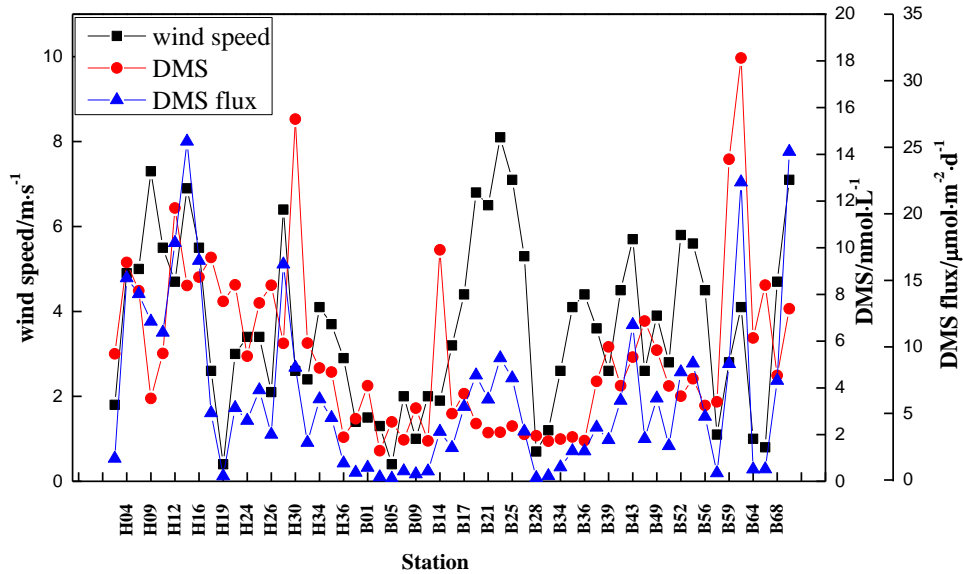
690

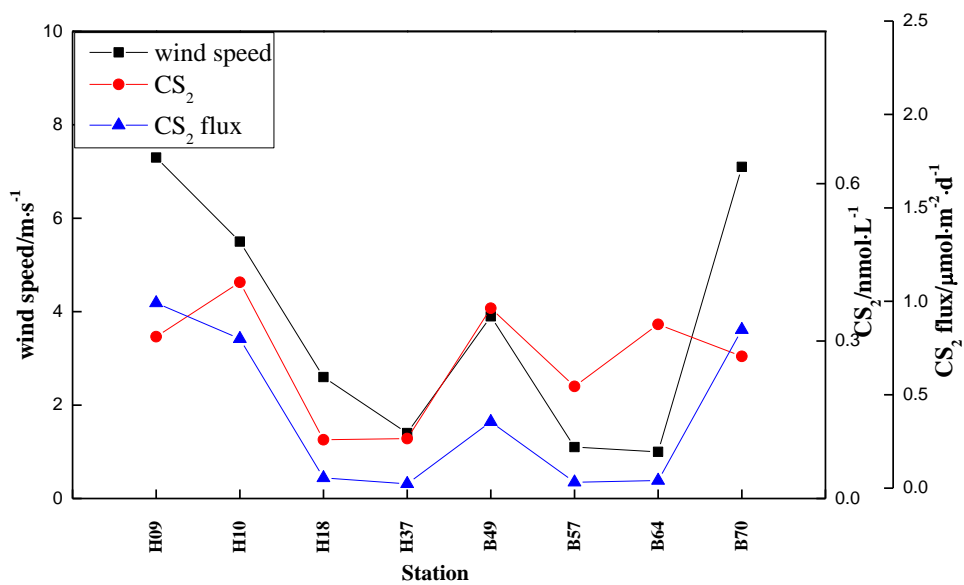**Fig. 7.** Variations in sea-to-air fluxes of VSCs, VSCs concentrations in seawater, and wind speeds in the BS and YS in spring 2018.

694

695

696

697

Fig. 8. Variations in sea-to-air fluxes of VSCs, VSCs concentrations in seawater, and wind speeds in the BS and YS

699   in summer 2018.

700 **Table 1** Correlation analyses of the three VSCs and environmental factors in the BS and YS in spring and summer.

Spring	COS (seawater)	DMS (seawater)	CS_2 (seawater)	COS (atmosphere)	DMS (atmosphere)	CS_2 (atmosphere)
COS (seawater)	1					
DMS (seawater)	0.021	1				
CS_2 (seawater)	0.193	0.281*	1			
COS (atmosphere)	-0.246	-0.355	-0.182	1		
DMS (atmosphere)	0.296	0.04	0.274	0.117	1	
CS_2 (atmosphere)	-0.201	-0.264	-0.213	0.554**	-0.013	1
Chl *a*	0.132	0.044	-0.095	0.033	0.179	-0.141
Temperature	0.286*	0.082	0.319**	-0.257	0.179	-0.372
Salinity	0.11	-0.009	-0.109	0.24	0.019	0.236
Silicate	-0.103	-0.252*	-0.029	0.351	-0.008	0.54
Phosphate	-0.084	-0.205	-0.353**	0.621	-0.128	0.36
Nitrate	-0.299*	-0.293*	-0.226	0.075	-0.096	0.044
DOC	-0.146	-0.153	-0.073	0.037	-0.122	0.008
Summer	COS (seawater)	DMS (seawater)	CS_2 (seawater)	COS (atmosphere)	DMS (atmosphere)	CS_2 (atmosphere)
COS (seawater)	1					
DMS (seawater)	0.009	1				
CS_2 (seawater)	-0.007	0.424**	1			
COS (atmosphere)	0.358	0.472	0.184	1		
DMS (atmosphere)	-0.266	0.404	0.31	0.451	1	
CS_2 (atmosphere)	0.452	0.229	0.424	0.855**	0.251	1
Chl *a*	-0.059	0.25	0.274*	0.461	-0.294	0.565
Temperature	0.088	-0.076	-0.143	-0.097	-0.349	0.072
Salinity	0.128	-0.172	-0.143	-0.12	-0.352	-0.044
Silicate	0.114	0.122	0.276*	0.312	-0.548	0.377
Phosphate	0.104	-0.169	-0.245	-0.49	-0.539	-0.482
Nitrate	-0.095	0.145	0.057	-0.008	0.224	-0.155
DOC	0.342*	-0.015	0.012	0.02	0.924	0.319

701 * indicates $P < 0.05$, ** indicates $P < 0.01$.